EUROPEAN ORGANIZATION FOR NUCLEAR RESEARCH

CERN–PPE/94-130

4 August 1994

Production Characteristics of K^0 and Light Meson Resonances in Hadronic Decays of the Z^0

DELPHI Collaboration

Abstract

An analysis of inclusive production of K^0 and the meson resonances $K^{*\pm}(892)$, $\rho^0(770)$, $f_0(975)$ and $f_2(1270)$ in hadronic decays of the Z^0 is presented, based on about 973,000 multihadronic events collected by the DELPHI detector at LEP during 1991 and 1992. Overall multiplicities have been determined as 1.962 ± 0.060 K^0 mesons, 0.712 ± 0.067 $K^{*\pm}(892)$ and 1.21 ± 0.15 $\rho^0(770)$ per hadronic Z^0 decay. The average multiplicities of $f_0(975)$ for scaled momentum, $x_p = p/p_{beam}$, in the range $0.05 \leq x_p \leq 0.6$ and of $f_2(1270)$ for $0.05 \leq x_p \leq 1.0$ are 0.098 ± 0.016 and 0.170 ± 0.043 respectively. The $f_0(975)$ and $\rho^0(770)$ x_p-spectra have similar shapes. The $f_2(1270)/\rho^0(770)$ ratio increases with x_p. The average multiplicities and the differential cross sections are compared with the JETSET Parton Shower model. The model with default parameters fails to reproduce the experimental K^0 momentum spectrum at low momentum, describes the $K^{*\pm}(892)$ and $\rho^0(770)$ x_p-spectrum shapes, but significantly overestimates their production rates.

(To be submitted to Zeit. f. Phys. C)

P.Abreu[20], W.Adam[7], T.Adye[37], E.Agasi[30], I.Ajinenko[42], R.Aleksan[39], G.D.Alekseev[14], P.P.Allport[21], S.Almehed[23], F.M.L.Almeida[47], S.J.Alvsvaag[4], U.Amaldi[7], A.Andreazza[27], P.Antilogus[24], V.Anykeyev[42], W-D.Apel[15], R.J.Apsimon[37], Y.Arnoud[39], B.Åsman[44], J-E.Augustin[18], A.Augustinus[30], P.Baillon[7], P.Bambade[18], F.Barao[20], R.Barate[12], G.Barbiellini[46], D.Y.Bardin[14], G.J.Barker[34], A.Baroncelli[40], O.Barring[7], J.A.Barrio[25], W.Bartl[50], M.J.Bates[37], M.Battaglia[13], M.Baubillier[22], J.Baudot[39], K-H.Becks[52], M.Begalli[36], P.Beilliere[6], P.Beltran[9], A.C.Benvenuti[5], M.Berggren[41], D.Bertrand[2], F.Bianchi[45], M.Bigi[45], M.S.Bilenky[14], P.Billoir[22], J.Bjarne[23], D.Bloch[8], J.Blocki[51], S.Blyth[34], V.Bocci[38], P.N.Bogolubov[14], T.Bolognese[39], M.Bonesini[27], W.Bonivento[27], P.S.L.Booth[21], G.Borisov[42], C.Bosio[40], B.Bostjancic[43], S.Bosworth[34], O.Botner[48], E.Boudinov[42], B.Bouquet[18], C.Bourdarios[18], T.J.V.Bowcock[21], M.Bozzo[11], S.Braibant[2], P.Branchini[40], K.D.Brand[35], R.A.Brenner[13], H.Briand[22], C.Bricman[2], L.Brillault[22], R.C.A.Brown[7], P.Bruckman[16], J-M.Brunet[6], L.Bugge[32], T.Buran[32], A.Buys[7], J.A.M.A.Buytaert[7], M.Caccia[27], M.Calvi[27], A.J.Camacho Rozas[41], R.Campion[21], T.Camporesi[7], V.Canale[38], K.Cankocak[44], F.Cao[2], F.Carena[7], P.Carrilho[47], L.Carroll[21], R.Cases[49], C.Caso[11], M.V.Castillo Gimenez[49], A.Cattai[7], F.R.Cavallo[5], L.Cerrito[38], V.Chabaud[7], A.Chan[1], M.Chapkin[42], Ph.Charpentier[7], L.Chaussard[24], J.Chauveau[22], P.Checchia[35], G.A.Chelkov[14], P.Chliapnikov[42], V.Chorowicz[22], J.T.M.Chrin[49], V.Cindro[43], P.Collins[34], J.L.Contreras[18], R.Contri[11], E.Cortina[49], G.Cosme[18], F.Couchot[18], H.B.Crawley[1], D.Crennell[37], G.Crosetti[11], J.Cuevas Maestro[33], S.Czellar[13], E.Dahl-Jensen[28], J.Dahm[52], B.Dalmagne[18], M.Dam[32], G.Damgaard[28], E.Daubie[2], A.Daum[15], P.D.Dauncey[37], M.Davenport[7], J.Davies[21], W.Da Silva[22], C.Defoix[6], P.Delpierre[26], N.Demaria[34], A.De Angelis[7], H.De Boeck[2], W.De Boer[15], S.De Brabandere[2], C.De Clercq[2], M.D.M.De Fez Laso[49], C.De La Vaissiere[22], B.De Lotto[46], A.De Min[27], L.De Paula[47], C.De Saint-Jean[39], H.Dijkstra[7], L.Di Ciaccio[38], F.Djama[8], J.Dolbeau[6], M.Donszelmann[7], K.Doroba[51], M.Dracos[8], J.Drees[52], M.Dris[31], Y.Dufour[7], F.Dupont[12], D.Edsall[1], R.Ehret[15], T.Ekelof[48], G.Ekspong[44], M.Elsing[52], J-P.Engel[8], N.Ershaidat[22], M.Espirito Santo[20], D.Fassouliotis[31], M.Feindt[7], A.Ferrer[49], T.A.Filippas[31], A.Firestone[1], H.Foeth[7], E.Fokitis[31], F.Fontanelli[11], F.Formenti[7], J-L.Fousset[26], B.Franek[37], P.Frenkiel[6], D.C.Fries[15], A.G.Frodesen[4], R.Fruhwirth[50], F.Fulda-Quenzer[18], H.Furstenau[7], J.Fuster[7], D.Gamba[45], M.Gandelman[17], C.Garcia[49], J.Garcia[41], C.Gaspar[7], U.Gasparini[35], Ph.Gavillet[7], E.N.Gazis[31], D.Gele[8], J-P.Gerber[8], P.Giacomelli[7], D.Gillespie[7], R.Gokieli[51], B.Golob[43], V.M.Golovatyuk[14], J.J.Gomez Y Cadenas[7], G.Gopal[37], L.Gorn[1], M.Gorski[51], V.Gracco[11], F.Grard[2], E.Graziani[40], G.Grosdidier[18], P.Gunnarsson[44], J.Guy[37], U.Haedinger[15], F.Hahn[52], M.Hahn[44], S.Hahn[52], S.Haider[30], Z.Hajduk[16], A.Hakansson[23], A.Hallgren[48], K.Hamacher[52], W.Hao[30], F.J.Harris[34], V.Hedberg[23], R.Henriques[20], J.J.Hernandez[49], J.A.Hernando[49], P.Herquet[2], H.Herr[7], T.L.Hessing[21], E.Higon[49], H.J.Hilke[7], T.S.Hill[1], S-O.Holmgren[44], P.J.Holt[34], D.Holthuizen[30], P.F.Honore[6], M.Houlden[21], J.Hrubec[50], K.Huet[2], K.Hultqvist[44], P.Ioannou[3], P-S.Iversen[4], J.N.Jackson[21], R.Jacobsson[44], P.Jalocha[16], G.Jarlskog[23], P.Jarry[39], B.Jean-Marie[18], E.K.Johansson[44], M.Jonker[7], L.Jonsson[23], P.Juillot[8], M.Kaiser[15], G.Kalmus[37], F.Kapusta[22], M.Karlsson[44], E.Karvelas[9], S.Katsanevas[3], E.C.Katsoufis[31], R.Keranen[7], B.A.Khomenko[14], N.N.Khovanski[14], B.King[21], N.J.Kjaer[28], H.Klein[7], A.Klovning[4], P.Kluit[30], A.Koch-Mehrin[52], J.H.Koehne[15], B.Koene[30], P.Kokkinias[9], M.Koratzinos[32], A.V.Korytov[14], V.Kostioukhine[42], C.Kourkoumelis[3], O.Kouznetsov[14], P.H.Kramer[52], M.Krammer[50], C.Kreuter[15], J.Krolikowski[51], I.Kronkvist[23], W.Krupinski[16], W.Kucewicz[16], K.Kulka[48], K.Kurvinen[13], C.Lacasta[49], I.Laktineh[24], C.Lambropoulos[9], J.W.Lamsa[1], L.Lanceri[46], P.Langefeld[52], V.Lapin[42], I.Last[21], J-P.Laugier[39], R.Lauhakangas[13], G.Leder[50], F.Ledroit[12], R.Leitner[29], Y.Lemoigne[39], J.Lemonne[2], G.Lenzen[52], V.Lepeltier[18], J.M.Levy[8], E.Lieb[52], R.Lindner[52], A.Lipniacka[18], I.Lippi[35], B.Loerstad[23], M.Lokajicek[10], J.G.Loken[34], A.Lopez-Fernandez[7], M.A.Lopez Aguera[41], M.Los[30], D.Loukas[9], J.J.Lozano[49], P.Lutz[39], L.Lyons[34], G.Maehlum[15], J.Maillard[6], A.Maio[20], A.Maltezos[9], F.Mandl[50], J.Marco[41], B.Marechal[47], M.Margoni[35], J-C.Marin[7], C.Mariotti[40], A.Markou[9], T.Maron[52], S.Marti[49], C.Martinez-Rivero[41], F.Martinez-Vidal[49], F.Matorras[41], C.Matteuzzi[27], G.Matthiae[38], M.Mazzucato[35], M.Mc Cubbin[21], R.Mc Kay[1], R.Mc Nulty[21], J.Medbo[48], C.Meroni[27], W.T.Meyer[1], M.Michelotto[35], E.Migliore[45], I.Mikulec[50], L.Mirabito[24], W.A.Mitaroff[50], G.V.Mitselmakher[14], U.Mjoernmark[23], T.Moa[44], R.Moeller[28], K.Moenig[7], M.R.Monge[11], P.Morettini[11], H.Mueller[15], W.J.Murray[37], B.Muryn[16], G.Myatt[34], F.Naraghi[12], F.L.Navarria[5], P.Negri[27], S.Nemecek[10], W.Neumann[52], N.Neumeister[50], R.Nicolaidou[3], B.S.Nielsen[28], P.Niss[44], A.Nomerotski[35], A.Normand[34], M.Novak[10], V.Obraztsov[42], A.G.Olshevski[14], R.Orava[13], K.Osterberg[13], A.Ouraou[39], P.Paganini[18], M.Paganoni[27], R.Pain[22], H.Palka[16], Th.D.Papadopoulou[31], L.Pape[7], F.Parodi[11], A.Passeri[40], M.Pegoraro[35], J.Pennanen[13], L.Peralta[20], H.Pernegger[50], M.Pernicka[50], A.Perrotta[5], C.Petridou[46], A.Petrolini[11], H.T.Phillips[37], G.Piana[11], F.Pierre[39], M.Pimenta[20], S.Plaszczynski[18], O.Podobrin[15], M.E.Pol[17], G.Polok[16], P.Poropat[46], V.Pozdniakov[14], M.Prest[46], P.Privitera[38], A.Pullia[27], D.Radojicic[34], S.Ragazzi[27], H.Rahmani[31], P.N.Ratoff[19], A.L.Read[32], M.Reale[52], P.Rebecchi[18], N.G.Redaelli[27], M.Regler[50], D.Reid[7], P.B.Renton[34], L.K.Resvanis[3], F.Richard[18], J.Richardson[21], J.Ridky[10], G.Rinaudo[45], I.Ripp[39], A.Romero[45], I.Roncagliolo[11], P.Ronchese[35], L.Roos[12], E.I.Rosenberg[1], E.Rosso[7], P.Roudeau[18], T.Rovelli[5], W.Ruckstuhl[30], V.Ruhlmann-Kleider[39], A.Ruiz[41], H.Saarikko[13], Y.Sacquin[39], G.Sajot[12], J.Salt[49], J.Sanchez[25], M.Sannino[11],

S.Schael[7], H.Schneider[15], M.A.E.Schyns[52], G.Sciolla[45], F.Scuri[46], A.M.Segar[34], A.Seitz[15], R.Sekulin[37], M.Sessa[46], R.Seufert[15], R.C.Shellard[36], I.Siccama[30], P.Siegrist[39], S.Simonetti[39], F.Simonetto[35], A.N.Sisakian[14], T.B.Skaali[32], G.Smadja[24], N.Smirnov[42], O.Smirnova[14], G.R.Smith[37], R.Sosnowski[51], D.Souza-Santos[36], T.Spassov[20], E.Spiriti[40], S.Squarcia[11], H.Staeck[52], C.Stanescu[40], S.Stapnes[32], I.Stavitski[35], G.Stavropoulos[9], K.Stepaniak[51], F.Stichelbaut[7], A.Stocchi[18], J.Strauss[50], J.Straver[7], R.Strub[8], B.Stugu[4], M.Szczekowski[51], M.Szeptycka[51], T.Tabarelli[27], O.Tchikilev[42], G.E.Theodosiou[9], Z.Thome[47], A.Tilquin[26], J.Timmermans[30], V.G.Timofeev[14], L.G.Tkatchev[14], T.Todorov[8], D.Z.Toet[30], A.Tomaradze[2], B.Tome[20], E.Torassa[45], L.Tortora[40], G.Transtromer[23], D.Treille[7], W.Trischuk[7], G.Tristram[6], C.Troncon[27], A.Tsirou[7], E.N.Tsyganov[14], M-L.Turluer[39], T.Tuuva[13], I.A.Tyapkin[22], M.Tyndel[37], S.Tzamarias[21], B.Ueberschaer[52], S.Ueberschaer[52], O.Ullaland[7], V.Uvarov[42], G.Valenti[5], E.Vallazza[7], J.A.Valls Ferrer[49], C.Vander Velde[2], G.W.Van Apeldoorn[30], P.Van Dam[30], M.Van Der Heijden[30], W.K.Van Doninck[2], J.Van Eldik[30], P.Vaz[7], G.Vegni[27], L.Ventura[35], W.Venus[37], F.Verbeure[2], M.Verlato[35], L.S.Vertogradov[14], D.Vilanova[39], P.Vincent[24], L.Vitale[46], E.Vlasov[42], A.S.Vodopyanov[14], M.Vollmer[52], M.Voutilainen[13], V.Vrba[10], H.Wahlen[52], C.Walck[44], F.Waldner[46], A.Wehr[52], M.Weierstall[52], P.Weilhammer[7], A.M.Wetherell[7], J.H.Wickens[2], M.Wielers[15], G.R.Wilkinson[34], W.S.C.Williams[34], M.Winter[8], M.Witek[7], G.Wormser[18], K.Woschnagg[48], K.Yip[34], F.Zach[24], A.Zaitsev[42], A.Zalewska[16], P.Zalewski[51], D.Zavrtanik[43], E.Zevgolatakos[9], V.Zhigunov[42], N.I.Zimin[14], M.Zito[39], D.Zontar[43], R.Zuberi[34], G.Zumerle[35]

[1] Ames Laboratory and Department of Physics, Iowa State University, Ames IA 50011, USA
[2] Physics Department, Univ. Instelling Antwerpen, Universiteitsplein 1, B-2610 Wilrijk, Belgium
and IIHE, ULB-VUB, Pleinlaan 2, B-1050 Brussels, Belgium
and Faculté des Sciences, Univ. de l'Etat Mons, Av. Maistriau 19, B-7000 Mons, Belgium
[3] Physics Laboratory, University of Athens, Solonos Str. 104, GR-10680 Athens, Greece
[4] Department of Physics, University of Bergen, Allégaten 55, N-5007 Bergen, Norway
[5] Dipartimento di Fisica, Università di Bologna and INFN, Via Irnerio 46, I-40126 Bologna, Italy
[6] Collège de France, Lab. de Physique Corpusculaire, IN2P3-CNRS, F-75231 Paris Cedex 05, France
[7] CERN, CH-1211 Geneva 23, Switzerland
[8] Centre de Recherche Nucléaire, IN2P3 - CNRS/ULP - BP20, F-67037 Strasbourg Cedex, France
[9] Institute of Nuclear Physics, N.C.S.R. Demokritos, P.O. Box 60228, GR-15310 Athens, Greece
[10] FZU, Inst. of Physics of the C.A.S. High Energy Physics Division, Na Slovance 2, 180 40, Praha 8, Czech Republic
[11] Dipartimento di Fisica, Università di Genova and INFN, Via Dodecaneso 33, I-16146 Genova, Italy
[12] Institut des Sciences Nucléaires, IN2P3-CNRS, Université de Grenoble 1, F-38026 Grenoble Cedex, France
[13] Research Institute for High Energy Physics, SEFT, P.O. Box 9, FIN-00014 Helsinki, Finland
[14] Joint Institute for Nuclear Research, Dubna, Head Post Office, P.O. Box 79, 101 000 Moscow, Russian Federation
[15] Institut für Experimentelle Kernphysik, Universität Karlsruhe, Postfach 6980, D-76128 Karlsruhe, Germany
[16] High Energy Physics Laboratory, Institute of Nuclear Physics, Ul. Kawiory 26a, PL-30055 Krakow 30, Poland
[17] Centro Brasileiro de Pesquisas Físicas, rua Xavier Sigaud 150, BR-22290 Rio de Janeiro, Brazil
[18] Université de Paris-Sud, Lab. de l'Accélérateur Linéaire, IN2P3-CNRS, Bat 200, F-91405 Orsay Cedex, France
[19] School of Physics and Materials, University of Lancaster, Lancaster LA1 4YB, UK
[20] LIP, IST, FCUL - Av. Elias Garcia, 14-1°, P-1000 Lisboa Codex, Portugal
[21] Department of Physics, University of Liverpool, P.O. Box 147, Liverpool L69 3BX, UK
[22] LPNHE, IN2P3-CNRS, Universités Paris VI et VII, Tour 33 (RdC), 4 place Jussieu, F-75252 Paris Cedex 05, France
[23] Department of Physics, University of Lund, Sölvegatan 14, S-22363 Lund, Sweden
[24] Université Claude Bernard de Lyon, IPNL, IN2P3-CNRS, F-69622 Villeurbanne Cedex, France
[25] Universidad Complutense, Avda. Complutense s/n, E-28040 Madrid, Spain
[26] Univ. d'Aix - Marseille II - CPP, IN2P3-CNRS, F-13288 Marseille Cedex 09, France
[27] Dipartimento di Fisica, Università di Milano and INFN, Via Celoria 16, I-20133 Milan, Italy
[28] Niels Bohr Institute, Blegdamsvej 17, DK-2100 Copenhagen 0, Denmark
[29] NC, Nuclear Centre of MFF, Charles University, Areal MFF, V Holesovickach 2, 180 00, Praha 8, Czech Republic
[30] NIKHEF-H, Postbus 41882, NL-1009 DB Amsterdam, The Netherlands
[31] National Technical University, Physics Department, Zografou Campus, GR-15773 Athens, Greece
[32] Physics Department, University of Oslo, Blindern, N-1000 Oslo 3, Norway
[33] Dpto. Fisica, Univ. Oviedo, C/P. Pérez Casas, S/N-33006 Oviedo, Spain
[34] Department of Physics, University of Oxford, Keble Road, Oxford OX1 3RH, UK
[35] Dipartimento di Fisica, Università di Padova and INFN, Via Marzolo 8, I-35131 Padua, Italy
[36] Depto. de Fisica, Pontificia Univ. Católica, C.P. 38071 RJ-22453 Rio de Janeiro, Brazil
[37] Rutherford Appleton Laboratory, Chilton, Didcot OX11 OQX, UK
[38] Dipartimento di Fisica, Università di Roma II and INFN, Tor Vergata, I-00173 Rome, Italy
[39] Centre d'Etude de Saclay, DSM/DAPNIA, F-91191 Gif-sur-Yvette Cedex, France
[40] Istituto Superiore di Sanità, Ist. Naz. di Fisica Nucl. (INFN), Viale Regina Elena 299, I-00161 Rome, Italy
[41] C.E.A.F.M., C.S.I.C. - Univ. Cantabria, Avda. los Castros, S/N-39006 Santander, Spain, (CICYT-AEN93-0832)
[42] Inst. for High Energy Physics, Serpukov P.O. Box 35, Protvino, (Moscow Region), Russian Federation
[43] J. Stefan Institute and Department of Physics, University of Ljubljana, Jamova 39, SI-61000 Ljubljana, Slovenia
[44] Fysikum, Stockholm University, Box 6730, S-113 85 Stockholm, Sweden
[45] Dipartimento di Fisica Sperimentale, Università di Torino and INFN, Via P. Giuria 1, I-10125 Turin, Italy
[46] Dipartimento di Fisica, Università di Trieste and INFN, Via A. Valerio 2, I-34127 Trieste, Italy
and Istituto di Fisica, Università di Udine, I-33100 Udine, Italy
[47] Univ. Federal do Rio de Janeiro, C.P. 68528 Cidade Univ., Ilha do Fundão BR-21945-970 Rio de Janeiro, Brazil
[48] Department of Radiation Sciences, University of Uppsala, P.O. Box 535, S-751 21 Uppsala, Sweden
[49] IFIC, Valencia-CSIC, and D.F.A.M.N., U. de Valencia, Avda. Dr. Moliner 50, E-46100 Burjassot (Valencia), Spain
[50] Institut für Hochenergiephysik, Österr. Akad. d. Wissensch., Nikolsdorfergasse 18, A-1050 Vienna, Austria
[51] Inst. Nuclear Studies and University of Warsaw, Ul. Hoza 69, PL-00681 Warsaw, Poland
[52] Fachbereich Physik, University of Wuppertal, Postfach 100 127, D-42097 Wuppertal 1, Germany

1 Introduction

Hadron production in Z^0 decays proceeds through two main steps : parton shower development from the primary $q\bar{q}$ pair produced from the Z^0, followed by fragmentation of the coloured partons into colorless hadrons. The first step is well described by QCD, the theory of strong interactions. However, perturbative QCD is not applicable to the soft processes of hadronization. The formation of hadrons out of quarks and gluons has been studied in many experiments in an attempt to understand the hadronization process better and to test phenomenological models of parton fragmentation. The most successful of these models are the string [1] and the cluster fragmentation [2] models. Studies of inclusive resonance production are particularly interesting because the resonances provide more direct information on the relative production rates of states differing in their flavour and spin composition, which may serve as guidelines for future development of the models. The role of mesons with non-zero angular momentum between the quarks, for example $f_0(975)$ and $f_2(1270)$, is of special interest in view of possible different dynamics of their production. Phenomenological consequences of the Gribov idea [3] that the $f_0(975)$ and $a_0(980)$ may play a special role in the dynamics of quark confinement are discussed in [4]. The production rate of high mass mesons can also affect the relative yields of the pseudoscalar and vector mesons.

Inclusive resonance production has been intensively studied in hadronic reactions (see, for example, [5,6] and refs. therein). With few exceptions, the data on resonance production in e^+e^- annihilation at energies below the Z^0 pole [7]-[14] suffer from poor statistical precision. More precise information is expected from the LEP experiments (with at least 5,000,000 hadronic Z^0 decays expected to be accumulated in each of them by the end of the LEP 100 program), although some problems exist because of the large combinatorial backgrounds due to the high multiplicities of hadronic Z^0 decays and the distortion of the resonance Breit-Wigner shapes in the $\pi^+\pi^-$ mass spectra by residual Bose-Einstein correlations.

Previous studies at LEP have presented analyses of the inclusive production of various meson resonances[†], including η and η' [15,16], $\rho^0(770)$, $f_0(975)$, $f_2(1270)$ [17], $\phi(1020)$ [18], $K^{*\pm}(892)$ [19,20] and $K^{*0}(892)$ [17,18]. This paper updates the results of refs. [17,18] on K^0, $K^{*\pm}(892)$, ρ^0, $f_0(975)$ and $f_2(1270)$ inclusive production. The data samples used were collected by the DELPHI experiment at LEP during 1991 and 1992 at centre-of-mass energies around 91.3 GeV. They contain about 1 million hadronic Z^0 decays in total.

The paper is organized as follows. The selection of charged particles, hadronic events and K^0_S is described in Section 2. The allowance for the restricted detector acceptance and efficiencies, and for finite experimental resolution by the least squares method is described in Section 3. Section 4 contains an account of the fitting procedure used and of effects due to particle misidentification. The treatment of residual Bose-Einstein correlations is described in Section 5, where the experimental results are presented. Comparison of the results with the JETSET model [21], discussion and conclusions are given in Section 6.

[†]Unless otherwise stated, antiparticles are implicitly included.

2 Event, charged particle and K^0_S selection

A detailed description of the DELPHI detector can be found in ref. [22]. Here, only the specific properties relevant to the present analysis are summarized.

The charged particle tracks were measured in the 1.2 T magnetic field by the following set of five tracking detectors:

- The Micro Vertex Detector (VD), which consisted of 3 layers of silicon, at radii, R, of 6.3, 9.0 and 11.0 cm. They measure $R\phi$ coordinates (in the plane transverse to the beam) over a length of 24 cm along the beam. The polar angle θ coverage of the VD is from 42° to 138°.
- The Inner Detector (ID) is a cylindrical drift chamber with inner and outer radii of 12 and 22 cm, covering polar angles between 29° and 151°.
- The Time Projection Chamber (TPC), the principal tracking device of DELPHI, is a cylinder with inner and outer radii of 30 cm and 122 cm and with a length of 2.7 m. Each end-cap is divided into 6 sector plates, each with 192 sense wires. The polar angle coverage of the TPC is from 20° to 160°
- The Outer Detector (OD) consists of 5 layers of drift cells at radii between 192 cm and 208 cm, covering polar angles between 43° and 137°.
- The Forward Chambers A and B (FCA and FCB) both cover polar angles between 11° and 33° and between 147° and 169°.

The average momentum resolution for charged particles in hadronic final states is in the range $\Delta p/p \simeq 0.001p$ to $0.01p$ (p in GeV/c), depending on which detectors are included in the track fit.

A charged particle is required to satisfy the following criteria :

- momentum greater than 0.2 GeV/c;
- $\Delta p/p < 1$;
- θ between 25° and 155°;
- measured track length in the TPC greater than 50 cm;
- impact parameter with respect to the nominal beam crossing point within 5 cm in the transverse (xy) plane and 10 cm along the beam direction (z-axis).

Hadronic events from Z^0 decays are then selected if

- there are at least 5 charged particles;
- the total energy of charged particles (assuming a pion mass) in each of two hemispheres (θ above and below 90°) exceeds 3 GeV;
- the total energy of all charged particles is greater than 15 GeV;
- the polar angle of the sphericity axis is between 40° and 140°.

A total of 683,403 events satisfied these cuts. The contamination from events due to beam-gas scattering and to $\gamma\gamma$ interactions is estimated to be less than 0.1% and the background from $\tau^+\tau^-$ events to be less than 0.2% of the accepted events.

The samples selected with the above cuts will be referred to below as the ones with the weak cuts. However, in order to decrease the fraction of $\pi^+\pi^-$ pairs possibly originating from neutral decays (V^0) and secondary interactions and thus to ensure better signal-to-background ratios for resonances in the $\pi^+\pi^-$ invariant mass spectra, additional selection criteria have been applied. The intersection point for each accepted pair of oppositely charged particles was required to satisfy one of the following conditions:

a) in case of two intersections in the xy plane, the solution with the smaller separation in z was chosen provided that it was less than 1.5 cm;

b) in case of non-intersecting particles in the xy plane, the minimum distance between them in this plane had to be smaller than 1 cm and the separation in z smaller than 1.5 cm;

The distance between the intersection point thus defined and the primary vertex defined from the vertex fit was required to be smaller than 1 cm in the xy plane and 1.5 cm along the z direction.

The samples selected with these additional cuts will be referred to below as the ones with the strong cuts. The strong cuts were chosen using simulated events from DELSIM [23] (see Sect. 3) in such a way that the fraction of rejected particle combinations originating from the primary vertex was less than 10%.

The production cross section of K^0 was studied in the subsample of data taken during 1992. The K^0_S candidates were detected by their decay in flight into $\pi^+\pi^-$. Candidate V^0 decays in the selected sample of hadronic events were found by considering all pairs of oppositely charged particles. The vertex defined by each such pair was determined such that the χ^2 obtained from the distances of the vertex to the extrapolated tracks was minimized. The tracks were then refitted imposing the common vertex.

The V^0 decay vertex candidates were required to satisfy the following criteria:

- in the xy plane, the angle between the vector sum of the charged particle momenta and the line joining the primary to the secondary vertex was less than $(10 + 20/p_t)$ mrad, where p_t is the transverse momentum of the V^0 candidate relative to the beam axis, in GeV/c;
- the radial separation of the primary and secondary vertex in the xy plane was greater than four standard deviations;
- when the reconstructed decay point of the V^0 was beyond the VD radius, there were no signals in the VD consistent with association to the decay tracks;
- the probability of the χ^2 fit to the secondary vertex was larger than 0.01;
- the transverse momentum of each particle of the V^0 with respect to the line of flight was larger than 0.02 GeV/c.

The $\pi^+\pi^-$ and $p\pi^-$ ($\bar{p}\pi^+$) invariant masses (attributing the proton mass to the particle of larger momentum) for the candidates passing the cuts listed above were calculated. When a pair was consistent within three standard deviations with both K^0 and Λ ($\bar{\Lambda}$) hypotheses, the one with the smaller mass pull (the absolute value of mass shift with respect to the nominal mass divided by the overall resolution) was selected.

The production cross section of $\mathrm{K}^{*\pm}(892)$ was studied in the combined sample of data taken during 1991 and 1992 with the looser V^0 selection criteria:

- the same as a) or b) used for the strong cuts;
- the distance between the primary and candidate secondary vertex in the xy plane (D_{xy}) and along the z direction (D_z) had to be $1.5 \leq D_{xy} \leq 90$ cm and $D_z \leq 100$ cm;
- each particle was required to have transverse momentum greater than 105 MeV/c with respect to the sum of the charged particle momenta;
- the angle in the xy plane between the vector sum of the charged particle momenta and the line joining the primary and secondary vertices was smaller than 40 mrad.

To construct a $\mathrm{K}^{*\pm}(892)$ candidate, those K^0_S candidates with a reconstructed mass between 480 and 515 MeV/c^2 were passed through a $1C$-fit to adjust the K^0_S mass and to correct the K^0_S momentum. They were then combined with a third charged particle which was assumed to be a pion and was selected according to the criteria described

above. However stricter cuts on impact parameter (0.4 cm in xy plane and 3 cm in z axis) were applied to ensure that the charged particle originated from, or close to, the primary vertex.

The signal-to-background ratio for the $K^{*\pm}(892)$ in the $K^0_S\pi^\pm$ invariant mass spectrum is quite good, since the K^0_S has little background and the $K^{*\pm}(892)$ has a width of 50 MeV/c^2. Besides, complications present for the $\pi^+\pi^-$ mass spectra due to the reflections and the residual Bose-Einstein correlations (see Sects. 3-5) are less important here. Therefore, these data were analysed using the weak cuts, and the strong cuts served only to check the reliability of the corresponding procedure for the $\pi^+\pi^-$ mass spectra and to estimate the systematic uncertainties arising from the application of the different (strong or weak) cuts. For this, the additional selection criteria for the $K^0_S\pi^\pm$ pairs were chosen to be as similar as possible to the ones applied for $\pi^+\pi^-$ pairs: intersection points between the K^0_S line of flight and charged particle were required to satisfy the same conditions a) or b), while the distance between the intersection point and the primary vertex had to be smaller than 5 cm in the xy plane and 5 cm along the z direction.

3 Treatment of detector imperfections

The detector imperfections, such as limited geometrical acceptance, particle interactions in the detector material etc, and different kinematical cuts imposed for charged particles and event selections are often taken into account by correction factors calculated from simulated events. Then the corrected data are fitted by some analytical function in order to extract the signals from the background and/or to test some theoretical predictions. However, this method relies on the deconvolution of the detector imperfections from the data, a process which is very sensitive to any systematic errors in the simulation (see for example [24]). Therefore for this study of resonance production an approach less sensitive to the systematic errors was applied (as already used by DELPHI [25]). Here the theoretical expectations were smeared and then compared with the uncorrected experimental data.

In this approach, the parameter vector a of the function $f(M,a)$, which is assumed to describe the true distribution of variable M, is determined by the least squares method from the minimization of the function

$$\chi^2 = \sum_m (N_m - \bar{N}_m(a))^2/\sigma_m^2, \tag{1}$$

where N_m is the experimentally observed (raw) number of entries in the m-th histogram bin of the measured variable M (the invariant mass in our case), $\bar{N}_m(a)$ is the expectation value of N_m which depends on the unknown parameters a of the function $f(M,a)$ and $\sigma_m^2 = N_m + \sigma^2(\bar{N}_m)$, where $\sigma(\bar{N}_m)$ is the error of $\bar{N}_m$. The relation between $\bar{N}_m(a)$ and $f(M,a)$ is determined by the detector acceptance and by the various selection criteria used, i.e. the probability for a particle pair with invariant mass M to be recorded, and by the experimental resolution, i.e. the probability to observe the measured instead of the true M. It can be found using the simulated events from DELSIM [23] as described below.

In DELSIM, events were generated using the JETSET 7.3 PS program [21] with the DELPHI default parameters. The particles were followed through the detector and simulated digitizations obtained were processed with the same reconstruction programs as the experimental data. A sample of 940,000 events passed the charged particle and event selection criteria used for the data sample. The 1991 and 1992 simulations were kept

separate and were then combined in the same proportion as the real data. The four following samples of events generated by DELSIM were considered:

- the first reference sample (S_1) consists of charged particles (and charged particle pairs) generated by JETSET 7.3 PS with the "true" values of their parameters;
- the sample S_2 consists of those charged particle tracks in the sample S_1 which are unambiguously associated with the reconstructed charged particles in DELSIM. The set of coefficients $A_n = N_n^{S_2}/N_n^{S_1}$, where $N_n^{S_1}$ and $N_n^{S_2}$ are the numbers of entries in the n-th histogram bin of the variable M for the samples S_1 and S_2, characterizes the detector acceptance;
- the same charged particles as in the sample S_2, but taken with the reconstructed momentum values, form the sample S_3. The distributions in samples S_2 and S_3 are related by the equation $N_m^{S_3} = \sum_n S_{mn} N_n^{S_2}$ where the smearing matrix, S_{mn}, satisfying the normalization conditions $\sum_m S_{mn} = 1$, characterizes the experimental resolution;
- the sample S_4 consists of all reconstructed and selected particles at the DELSIM output. The vector $C_m = N_m^{S_4}/N_m^{S_3}$ characterizes losses of particles due to the selection criteria imposed and extra particles due to ghosts, secondary interactions etc., absent in the reference sample S_1.

Thus the relation between $\bar{N}_m(a)$ and $f_n(a) = \int_{M_n}^{M_{n+1}} f(M,a)\ \mathrm{d}M$, where M_n is the lower edge of n-th histogram bin of variable M, can be written as

$$\bar{N}_m(a) = C_m \sum_n S_{mn} A_n f_n(a). \tag{2}$$

The smearing matrices S_{mn} for the $\mathrm{K}^0_S\pi^\pm$ invariant mass distributions for the separate x_p-intervals are derived from the distributions presented in fig. 1. The matrices are approximately diagonal apart from an almost uniform background due to badly measured or wrongly associated charged particles. The width of the strip close to the diagonal characterizes the mass resolution, deteriorating as expected with increasing mass and scaled momentum. The smearing matrices for the $\pi^+\pi^-$ invariant mass distributions (not shown) exhibit similar behavior.

The coefficients A characterizing the detector acceptance are shown as a function of the $\mathrm{K}^0_S\pi^\pm$ and $\pi^+\pi^-$ invariant masses for the indicated x_p-intervals in figs. 2 and 3. By definition, they are the same for event samples with weak and strong cuts described in Sect. 2. This is not the case for the coefficients C for these two samples presented as a function of $\mathrm{K}^0_S\pi^\pm$ and $\pi^+\pi^-$ invariant masses in fig. 4 and 5. The coefficients C obtained with the weak cuts are close to 1 and exhibit a relatively smooth dependence on $M(K^0_S\pi^\pm)$, apart from the last two x_p-intervals (fig. 4). Clearly in this case an application of the strong cuts is not justified: they smoothen the $C(M)$ dependence in the last two x_p-intervals, but at the expense of a significant decrease of statistics. The situation is different for the coefficients C as a function of $M(\pi^+\pi^-)$. For the sample with the weak cuts, they are much larger than 1, especially in the low mass region at small x_p-values, thus showing that quite an important fraction of the particle pairs is contaminated by particles from the V^0 decays, secondary interactions and by wrongly associated charged particles, increasing the background in a very important way. Another feature is a significant irregularity in the low mass and low x_p regions. On the other hand, the coefficients C for the sample with the strong cuts are smaller than 1 and they exhibit a smooth dependence on $M(\pi^+\pi^-)$. For these reasons only the event sample with the strong cuts will be used in the following analysis of the $\pi^+\pi^-$ invariant mass distributions.

The weak (standard DELPHI) cuts were chosen to ensure that the average multiplicity for the data and events simulated by DELSIM was the same. But due to imperfections of the DELSIM tuning, the shapes of some of the distributions for the data and simulated events can be slightly different. In such cases, the integrals of these distributions for the data and simulated events can also be different if the strong cuts are applied. Indeed it was observed that the ratios of the $\pi^+\pi^-$ invariant mass distributions, $\mathrm{d}\sigma/\mathrm{d}M$, obtained for the samples with the strong and weak cuts are different for the data ($R_D(M)$) and simulated events ($R_S(M)$). To take this into account, the coefficients C were divided by the factor $R = R_D(M)/R_S(M)$ in each of the considered x_p-intervals. These factors were approximated by constants, since their dependence on M for $M \geq 0.6$ GeV/c^2 was relatively small, decreasing from $R = 1.13$ for $0.025 \leq x_p \leq 0.05$ to 1.09 for $0.6 \leq x_p \leq 1$. The variation of R with M was taken into account in calculating the systematic uncertainties of the resonance production rates.

In principle, the reconstruction efficiency for the resonance signals and the background can be different, due to different angular distributions. Therefore it was explicitly checked that this was not the case for the generated events.

4 Parameterization of invariant mass distributions

The resonance cross sections were obtained by analyzing the $\mathrm{K}^0_S\pi^\pm$ and $\pi^+\pi^-$ invariant mass distributions for the full measured x_p-range and for intervals of x_p. The resonance signals were described by a relativistic Breit-Wigner function

$$BW(M) = \frac{M \cdot M_0 \cdot \Gamma(M)}{(M_0^2 - M^2)^2 + (M_0 \cdot \Gamma(M))^2} \tag{3}$$

$$\Gamma(M) = \Gamma_0 \cdot \left(\frac{q}{q_0}\right)^{2L+1} \cdot \frac{2q_0^2}{q_0^2 + q^2}$$

with an angular momentum for decay products $L = 0$ for $f_0(975)$, $L = 1$ for ρ^0 and $\mathrm{K}^*(892)$, and $L = 2$ for $f_2(1270)$ and $\mathrm{K}^*_2(1430)$. M_0 and Γ_0 stand for the resonance mass and natural width; q_0 and q are momenta of decay products in the resonance c.m. system for masses M_0 and M respectively.

The background was described by the function

$$BG(M) = (M - M_{th})^{\alpha_1} \cdot exp(\alpha_2 M + \alpha_3 M^2 + \alpha_4 M^3), \tag{4}$$

where M_{th} is the threshold invariant mass of the decay products.

For the $\pi^+\pi^-$ invariant mass distribution, a wrong particle identification leads not only to an increased combinatorial background, but also to the problem of reflections when resonance signals in $\mathrm{K}^\pm\pi^\mp$ or $\mathrm{K}^+\mathrm{K}^-$ systems distort the $\pi^+\pi^-$ invariant mass spectrum.[‡] These reflections are particularly severe when relatively narrow resonances such as ρ^0 and $\mathrm{K}^{*0}(892)$ or $f_2(1270)$ and $\mathrm{K}^{*0}_2(1430)$ with comparable production cross sections overlap in phase space. This problem can however be solved, provided the statistics are large enough, taking the shapes of these reflections into the $\pi^+\pi^-$ mass spectrum from the simulated events and determining the corresponding cross sections from the fit.

In order to obtain analytical forms for the reflections in the $\pi^+\pi^-$ mass spectra with the resonance parameters M_0 and Γ_0 to be obtained from the fit and, in addition, in order to replace the non-relativistic Breit-Wigner shape of the $\mathrm{K}^{*0}(892)$ in JETSET by

[‡]The reflection from $\phi(1020)$ into the $\pi^+\pi^-$ mass distribution is broad and its contribution is small. Therefore it has been ignored.

the relativistic one, the following procedure was applied. For each generated $K^{*0}(892) \to K^{\pm}\pi^{\mp}$ decay, the pion mass was assigned to the K^+ or K^- and the matrix Q'_{ij} (with indexes i and j running through $M_{\pi\pi}$ and $M_{K\pi}$ masses respectively) was constructed (with one entry for each decay). The renormalized matrix

$$Q_{ij} = Q'_{ij} / \sum_i Q'_{ij}$$

is independent of the shape of the $K\pi$ mass distribution. The reflection function $RF(M_{\pi\pi})$, properly taking into account the relativistic Breit-Wigner shape of the $K^{*0}(892)$, was then obtained from the convolution

$$RF_i = \sum_j Q_{ij} BW_j, \tag{5}$$

where $BW(M_{K\pi})$ is taken as (3). No spin alignment for the $K^{*0}(892)$ was assumed (in principle, it can be allowed for by calculating the reflections separately for each term of the spin density matrix, with the values of the spin density matrix elements as free parameters).

Another type of distortion of the $\pi^+\pi^-$ mass spectrum arises from the decays of $\eta \to \pi^+\pi^- X$, $\eta' \to \pi^+\pi^- X$, $\omega(783) \to \pi^+\pi^- X$ and from the $K^0_S \to \pi^+\pi^-$ decays close to the primary vertex. They were treated in a straightforward way by taking the corresponding $\pi^+\pi^-$ invariant mass distributions from JETSET. Since the shapes of the $\pi^+\pi^-$ mass spectra from η and η' were found to be practically the same, the corresponding reflection functions were combined.

Thus the fit of the $\pi^+\pi^-$ invariant mass spectrum was performed with the function $f(M,a)$ in (2) in the form

$$\begin{aligned} f(M,a) &= a_1 BW_{\rho^0}(M,a_2,a_3) + a_4 BW_{f_0}(M,a_5,a_6) + a_7 BW_{f_2}(M,a_8,a_9) \\ &+ a_{10} RF_{K^{*0}}(M,a_{11},a_{12}) + a_{13} RF_{K^{*0}_2}(M,a_{14},a_{15}) \\ &+ a_{16}\delta(M - M_{K^0}) + a_{17} RF_{\eta/\eta'}(M) + a_{18} RF_{\omega}(M) + a_{19} BG(M,a_{20},...,a_{23}). \end{aligned} \tag{6}$$

Usually resonance masses M_0 (parameters a_2, a_5, a_8, a_{11} and a_{14} in (6)) and widths Γ_0 (parameters a_3, a_6, a_9, a_{12} and a_{15} in (6)) in fitting procedures are either left free or are fixed at their measured values or at the ones given in the PDG tables [26]. This latter procedure was used in this study, with one important modification: instead of leaving the resonance parameters fixed, they were weighted towards their nominal values by including extra terms in the χ^2:

$$\chi^2 = \sum_m (N_m - \bar{N}_m(a))^2/\sigma_m^2 + \sum_i (a_i - \bar{a}_i)^2/(\Delta\bar{a}_i)^2, \tag{7}$$

where the a_i in the second term are the running values of M_0 and/or Γ_0, and $\bar{a}_i \pm \Delta\bar{a}_i$ the corresponding fixed values of M_0 and/or Γ_0 with their errors taken from [26].

In order to reduce the correlations between fitted parameters, independent information from other experiments can be used for the reflections. These include the measured $K^{*\pm}(892)$ production rate obtained in this study and by OPAL [20] (together with an assumption about equal $K^{*\pm}(892)$ and $K^{*0}(892)$ production), the η and η' production rates measured by L3 [15,28] and ALEPH [16], and the relative ω/ρ^0 production rates measured by ARGUS [14] and in hadronic reactions [5,6] (see Sect. 5.3 for details). The corresponding terms were also included into the second term of function (7).

The assumption about equal $K^{*\pm}(892)$ and $K^{*0}(892)$ production rates is of special importance for a reliable determination of the ρ^0 production rate from the $\pi^+\pi^-$ mass

distribution, due to very strong distortion of the ρ^0 signal by the $K^{*0}(892)$ reflection. This is illustrated in fig. 6 for the ρ^0 signal and $K^{*0}(892)$ reflection in the $\pi^+\pi^-$ mass distribution for four intervals of $|\cos\theta^*|$, where θ^* is the angle between the momentum of the pion in the $\pi^+\pi^-$ c.m. system and flight direction of the $\pi^+\pi^-$ pair, using events generated by JETSET 7.4 PS. The ρ^0 signal and $K^{*0}(892)$ reflection practically overlap for $|\cos\theta^*| \geq 0.5$. A reasonable separation is seen only for $|\cos\theta^*| \leq 0.25$. Such strong overlapping results in a distortion of the experimentally observed ρ^0 signal and in particular in the shift of the observed ρ^0 peak position to lower mass in the real data. This implies that in the absence of particle identification the extraction of the ρ^0 signal from the $\pi^+\pi^-$ mass distribution is only possible (at least in the full $\cos\theta^*$ range) if the $K^{*0}(892)$ production rate is fixed at an independently measured value.

Similar arguments are also valid for the case of the $f_2(1270)$ production where the $K_2^{*0}(1430)$ reflection plays an even more important role. But unfortunately in this case the same procedure is almost useless due to a poorly measured $K_2^{*\pm}(1430)$ production rate. Therefore it was used only to estimate the corresponding systematic error for the $f_2(1270)$ production rate.

For the $K^0_S\pi^\pm$ invariant mass spectrum, there are no such complications. Therefore it was fitted using formulae (2)-(4) and (7) with the function $f(M,a)$ in (2) taken in the form

$$f(M,a) = a_1 BW_{K^{*\pm}}(M,a_2,a_3) + a_4 BW_{K_2^{*\pm}}(M,a_5,a_6) + a_7 BG(M,a_8,...,a_{11}), \qquad (8)$$

both with and without the $K_2^{*\pm}(1430)$.

The resonance cross sections were then determined by integrating the Breit-Wigner functions in expressions (6) or (8):

$$\sigma(res_i) = a_i \int BW_i(M)dM. \qquad (9)$$

5 Results

5.1 K^0 production

The $\pi^+\pi^-$ invariant mass spectrum for the accepted K^0_S candidates is shown in fig. 7. A clear K^0_S signal is seen, with a resolution of about 4.3 MeV/c^2. The peak corresponds to about 150,000 reconstructed K^0_S.

The momentum-dependent efficiency for K^0_S reconstruction, including detector acceptance effects, has been calculated by the detailed simulation. The combinatorial background was subtracted independently for each interval of $\xi = \ln(1/x_p)$, with bins as in table 1; the widths of the fitting functions were allowed to vary independently for each interval of ξ.

The fitted mass value in each ξ interval is practically constant, giving an average value of $M(K^0_S) = 497.73 \pm 0.03(\text{stat}) \pm 0.11(\text{syst})$ MeV/c^2, consistent with the world average of 497.67 ± 0.03 MeV/c^2 [26]. The systematic errors include:

- stability of the mass value over different intervals of ξ;
- contribution from using a Gaussian or a Breit-Wigner distribution for fitting the signal in each interval of ξ;
- dependence on the modelling of the energy loss in the reconstruction of charged particles. To estimate this effect, an amount of energy equal to $kLB(p)$ (where L is the amount of material crossed by the particle before entering the sensitive region

of the TPC (in units of radiation lengths), $B(p)$ is a parameterization of the Bethe-Bloch function for the relevant materials, and k was allowed to vary) was added to each candidate pion from the decay of K^0_S. The systematic contribution corresponds to the error (at one standard deviation) of the value of k minimizing the variance of the mass values (as a function of ξ) with respect to the average.

The above result cannot be taken as a measurement of the K^0_S mass, since the analysis procedure is biased towards the nominal K^0_S mass, because of the method used for the resolution of K^0/Λ ambiguity.

The resolution ΔM (in MeV/c^2) as a function of ξ was parameterized as $\Delta M(\xi) = 2.7 + 40.43 \exp(-0.94\xi)$.

The K^0_S lifetime, $\tau_{K^0_S}$, has been determined from the selected sample within $\pm 2\Delta M(\xi)$ of the nominal mass value. The correction factors for each bin of proper time are calculated from the simulation. A least-square fit of the corrected experimental distribution to an exponential decay function gives $\tau_{K^0_S} = 88.7 \pm 0.6$ ps (the error is statistical only), compared with the world average of 89.2 ± 0.2 ps [26].

The K^0_S signal in each bin of ξ was estimated in five ways:

1) by fitting the mass spectrum with a sum of a Gaussian plus a linear background;
2) by fitting the mass spectrum with a sum of a Breit-Wigner plus a linear background;
3) ,4)by smoothing the results of 1), 2) as a function of ξ with a function $a + G(\xi)$, where G is a Gaussian function;
5) by subtracting from the number of candidates in the mass interval ranging from 0.42 to 0.58 GeV/c^2 four times the sum of the number of candidates between 0.40 and 0.42 and between 0.58 and 0.60 GeV/c^2.

The reconstruction efficiency was then estimated by following the same procedure on simulation.

The differential cross section $(1/\sigma_h)\cdot \mathrm{d}\sigma/\mathrm{d}\xi$ and $(1/\sigma_h)\cdot \mathrm{d}\sigma/\mathrm{d}x_p$ (where σ_h is the total hadronic cross section) for inclusive K^0 production at the Z^0 is shown in table 1 and in fig. 8a and 8b. The errors on the differential cross section include both the statistical and the systematic contributions. The systematic error comes from:

- spread of the results obtained with the five ways of estimating the signal;
- a relative amount of 2% added to each bin to account for difference in χ^2 probability distributions for secondary vertices between the data and simulated events in DELSIM.

The average reconstruction efficiency (weighted over the different intervals of ξ) of $K^0_S \to \pi^+\pi^-$ decays was estimated by simulation to be about 36%.

The mean K^0 multiplicity was obtained by integrating the $(1/\sigma_h)\cdot \mathrm{d}\sigma/\mathrm{d}\xi$ distribution, correcting for the unseen decay modes and for K^0_L and assuming that the unmeasured regions of ξ contain the same fraction of K^0 as predicted by JETSET 7.4 PS. This gave

$$< N(K^0) > = 1.962 \pm 0.022(stat) \pm 0.056(syst). \qquad (10)$$

The systematic error reflects the uncertainties due to:

- the fitting function for the signal. The error due to this source was estimated to be ± 0.039;
- the JETSET 7.4 PS extrapolation. The average number of K^0 in the unobserved region is about 0.009 according to the simulation; the relative uncertainty on this number was set to 100%;

– an amount of 2% to account for different efficiencies for K^0_S from secondary decays.

The result is about 1.7 standard deviations lower than the previous determination by DELPHI [19] and agrees within errors with the values of 2.10 ± 0.02 ± 0.14, 2.04 ± 0.02 ± 0.14 and 2.06 ± 0.05 of the OPAL [27], L3 [28] and ALEPH [29] experiments respectively.

5.2 $K^{*\pm}(892)$ production

The measured $K^0_S\pi^\pm$ invariant mass distributions for several $x_p(K^0_S\pi^\pm)$-intervals and for the $x_p(K^0_S\pi^\pm) \geq 0.05$ range are shown in fig. 9. The signal due to $K^{*\pm}(892)$ is clearly observed with about 18,500 $K^{*\pm}(892)$ in the peak for $x_p \geq 0.05$. No clear evidence for $K^{*\pm}_2(1430)$ production is seen. Therefore the mass spectrum for $x_p \geq 0.05$ was first fitted with a single Breit-Wigner contribution (with variable M_0 and Γ_0) in the mass range between 0.64 and 1.44 GeV/c^2. The results of the fit were $M_0 = 893.9 \pm 1.4$ MeV/c^2 and $\Gamma_0 = 53 \pm 6$ MeV/c^2. These values agree within errors with the world mean values [26].

To obtain the $K^{*\pm}(892)$ differential cross section, $(1/\sigma_h)\cdot d\sigma/dx_p$, the fit was then repeated in each x_p-interval with the mass free and the width taken at the PDG value of 49.8 ± 0.8 MeV/c^2. The fits are presented in fig. 9. The fit describes the data very well, as seen from the χ^2/NDF values also shown in fig. 9.

In calculating the cross section, unobserved $K^{*\pm}(892)$ decay modes were taken into account. The differential cross sections obtained are tabulated in table 2 and also presented in fig. 8c, with the statistical and systematic errors combined quadratically.

The measured average $K^{*\pm}(892)$ multiplicity per hadronic event in the $0.05 \leq x_p \leq 0.6$ range obtained by integration of the x_p-spectrum amounted to

$$< N(K^{*\pm}(892)) > = 0.462 \pm 0.020(stat) \pm 0.021(syst) \qquad (11)$$

(and agrees with the value of $0.450 \pm 0.019(stat) \pm 0.022(syst)$ obtained from the fit of overall mass spectrum in the $x_p \geq 0.05$ range).

The first error in (11) is the statistical one obtained from the fit, the second is the systematic one. The latter was estimated by analyzing the systematic uncertainties arising from:

1) K^0_S selection criteria;
2) difference in cross sections obtained for the samples selected with the weak or strong cuts;
3) choice of the background parameterization, bin size of the mass spectra and mass range used in the fit.

The relative systematic error due to the K^0_S selection criteria was ±3%. The second contribution was evaluated by repeating the fits for the sample selected with the strong cuts. The measured average $K^{*\pm}(892)$ multiplicity in the $0.05 \leq x_p \leq 0.6$ range obtained by integration of the x_p-spectrum was found to be 0.478 ± 0.033(stat) with the width fixed at the PDG value, and 0.457 ± 0.047(stat) with variable width. From this the systematics accounting for the selection criteria used was found to be 3.5%. The third contribution was estimated by applying exactly the same fitting procedure to the events generated by DELSIM and selected in exactly the same way as the real data. This gave a relative error of 0.5%. Thus the total systematic error of 4.6% is dominantly determined by the first two factors.

Extrapolation to the full x_p-range, assuming the unmeasured regions are represented by the normalized JETSET 7.4 PS model and the 20% error of the extrapolation, gave

$$< N(K^{*\pm}(892)) > = 0.712 \pm 0.031(stat) \pm 0.032(syst) \pm 0.050(extr). \qquad (12)$$

The value (12) agrees within errors with the recent value of 0.72 ± 0.02 ± 0.08 of the OPAL experiment [20], but it is 2.3 standard deviations below the previous DELPHI estimate [19]. With the present analysis using 20 time larger statistics than were available in 1990, possible systematic effects are now better understood, so the current value (12) replaces the older one.

Repeating the fit in the $x_p \geq 0.05$ region with the $K_2^{*\pm}(1430)$ contribution included (with M_0 and Γ_0 taken at the PDG values) results in $< N(K_2^{*\pm}(1430)) > = 0.05 \pm^{0.07}_{0.05} (stat)$ where extrapolation to the unmeasured x_p-region is included. Clearly larger statistics are necessary for a reliable estimate of the $K_2^{*\pm}(1430)$ production rate.

5.3 Neutral meson resonance production

As has been discussed in Sect. 4, the correlations between parameters in function (7) used for fitting the $\pi^+\pi^-$ invariant mass distributions can be significantly reduced using the following experimental information:

1. Combining the result of this study on the $K^{*\pm}(892)$ production rate (12) with the OPAL result [20], the average $K^{*\pm}(892)$ multiplicity per hadronic Z^0 equals 0.715 ± 0.052. The relative ratio of the $K^{*0}(892)$ and $K^{*\pm}(892)$ production rates at LEP was assumed to be equal to the JETSET model estimate of 0.95. Therefore the average $K^{*0}(892)$ multiplicity was taken to be 0.68 ± 0.05.

2. The ω/ρ^0 ratio in hadronic K^+p and pp reactions at c.m. energies $\sqrt{s}$ = 22 and 27 GeV equals 1.01 ± 0.28 [5] and 1.02 ± 0.08 [6] respectively. ARGUS measured ω/ρ^0 = 0.91 ± 0.20 [14]. Therefore the ω/ρ^0 ratio was taken at the average value of 1.00 ± 0.07. This agrees with the JETSET model estimate of 0.94 at LEP energies, when the difference between the predicted and measured [16] η' multiplicity (see below) is taken into account.

3. The average η and η' multiplicities for $x_p \geq 0.1$ measured by ALEPH [16] are equal to 0.298 ± 0.023 ± 0.021 and 0.068 ± 0.018 ± 0.016 and the corresponding ratios of the measured and JETSET predicted values are equal to 0.90 ± 0.09 for η and 0.25 ± 0.08 for η'. The extrapolation to the full x_p-range was made according to the JETSET model assuming the same ratios in unmeasured x_p-regions. In fitting the $\pi^+\pi^-$ mass spectra in different x_p-intervals the JETSET model normalized to the values given above was used.

4. The masses and widths of the $K^{*0}(892)$, ρ^0, $f_0(975)$ and $f_2(1270)$, with their errors, were taken from the PDG tables [26], unless stated otherwise.

The measured $\pi^+\pi^-$ invariant mass distribution was first considered in the $|\cos\theta^*| \leq 0.25$ region, where the ρ^0 signal and $K^{*0}(892)$ reflections are reasonably well separated, and fitted in the $x_p \geq 0.025$ range with the variable ρ^0 mass and width using the procedure described in Sect. 4. The ρ^0 width thus obtained, $\Gamma_0 = 130 \pm 17$ MeV/c^2, was found to be compatible within error with the PDG value. Therefore the width was subsequently taken equal to $\Gamma_0 = 151.5 \pm 1.2$ MeV/c^2 [26] and the fit was repeated with the variable ρ^0 mass. The fitted ρ^0 mass was found to be 748 ± 3 MeV/c^2, shifted significantly in comparison with the PDG value of 768.1 ± 0.5 MeV/c^2, as has been also observed by OPAL [18].

As suggested in [18,30,31], this significant mass shift can be explained, at least partly, by distortion of the Breit-Wigner shape for oppositely charged particles by Bose-Einstein

correlations among the identical $\pi^+\pi^+$ or $\pi^-\pi^-$ pairs. This is expected to have a stronger influence at low momenta. The fact that no such shift for the ρ^0 mass was recently observed by ARGUS [14] or by other lower energy e^+e^- experiments [7,8,11] can be attributed [18] to increased multiplicity of pions which are close in phase space to the decay products of the ρ^0 at LEP energies. We therefore attempted to take residual Bose-Einstein correlations into account using the following ansatz.

The parameters a_1, a_4 and a_7 in expression (6) have been assumed so far to be constants. This is justified if the mass spectrum of non-resonant $\pi^+\pi^-$ pairs, representing the two-pion phase space distribution, $PS(M)$, is a slowly varying function of M, as compared to the $BW(M)$ dependence. If this is not the case, each Breit-Wigner term in (6) has to be replaced by $a_i PS_i(M) BW_i(M)$. If in addition Bose-Einstein effects are important, these terms have the form $a_i W_i(M) BW_i(M)$, where $W_i(M) = BE_i(M) PS_i(M)$ represents the effective phase space distribution modified by residual Bose-Einstein correlations, $BE(M)$. Then eq. (9) for the resonance cross section has to be replaced by

$$\sigma(res_i) = a_i \int PS_i(M) BW_i(M) dM$$

or

$$\sigma(res_i) = a_i \int W_i(M) BW_i(M) dM.$$

The functions $PS(M)$ and $W(M)$ for the ρ^0 and $f_2(1270)$ were obtained by generating the invariant mass distributions for the ρ^0 and $f_2(1270)$ using the JETSET 7.3 Parton Shower program without (for $PS(M)$) or with (for $W(M)$) Bose-Einstein correlations. Bose-Einstein correlations were included after the decay of short-lived resonances, but before decays of long-lived ones [21]. A Gaussian parameterization of the Bose-Einstein correlations with the parameters $\lambda = 1$ and $r = 0.5$ fm (describing, respectively, the correlation strength and the radius of the pion source) was used, which provided a reasonable description of the DELPHI data on like-sign and unlike-sign two-particle correlations [31] (with the experimentally determined values of $\lambda = 1.06 \pm 0.05 \pm 0.16$ and $r = 0.49 \pm 0.01 \pm 0.05$ fm). The functions $PS(M)$ and $W(M)$ were then calculated by dividing the generated mass distributions (normalized to 1) by the analytical $BW(M)$ functions used in JETSET (also normalized to 1).

The dependence of $PS_{\rho^0}(M)$ and $W_{\rho^0}(M)$ on $M - M_{\rho^0}$ is presented for several x_p-intervals in fig. 10. The dependence of $PS_{\rho^0}(M)$ in the ρ^0 mass region is important at the smallest x_p-interval, leading to some distortion of the ρ^0 Breit-Wigner shape even in absence of Bose-Einstein correlations, but it can be neglected for $x_p \geq 0.05$. $W_{\rho^0}(M)$ shows a sharp rise due to Bose-Einstein correlations for $M \leq M_{\rho^0}$, which is especially strong at the smallest x_p-values.[§] This effect, if ignored, clearly results in a shift of the central ρ^0 mass to a lower value, as observed.

For the $\pi^+\pi^-$ invariant mass distribution in the $|\cos\theta^*| \leq 0.25$ region and for the $x_p \geq 0.025$ range (fig. 11a, previously fitted using the unmodified function (6)), the fit with the fixed ρ^0 width and variable mass and with function (6) for the ρ^0 modified to take into account Bose-Einstein correlations now gives $M_{\rho^0} = 763.6 \pm 2.6$ MeV/c^2, compatible with the PDG value [26]. Thus it appears that the ρ^0 mass shift can indeed be explained by the Bose-Einstein correlations and can be corrected for by the proposed procedure.

The influence of Bose-Einstein correlations for the narrow $f_0(975)$ and $K^*(892)$, can be ignored. For the $f_2(1270)$, qualitatively similar dependences (not shown) were observed for the generated events with an even stronger effect than for the ρ^0. Thus, according to

[§] It is also of interest that W_{ρ^0} as a function of $M - M_{\rho^0}$ does not depend on the central ρ^0 mass value as has been checked by varying M_{ρ^0} by ± 60 MeV/c^2.

JETSET, the shift in the $f_2(1270)$ mass is as large as 77 MeV for $0.05 \leq x_p \leq 0.10$ and decreases with increasing x_p down to 19 MeV for $0.3 \leq x_p \leq 0.6$. However, the influence of Bose-Einstein correlations on the $f_2(1270)$ in the data is more difficult to see due to the smaller statistical significance of the signal.

Finally, the $\pi^+\pi^-$ invariant mass spectra integrated over all $\cos\theta^*$ were fitted in separate x_p-intervals with the resonance masses and widths fixed at their PDG values (according to the procedure described in Sect. 4) and with the modified function (6) for the ρ^0 and $f_2(1270)$.

The measured $\pi^+\pi^-$ invariant mass distributions in five x_p-intervals are presented in fig. 11b to f together with the results of the fits which describe the data quite well. Also shown are the separate contributions from $(\eta+\eta') \to \pi^+\pi^- X$, $\omega \to \pi^+\pi^- X$, $\mathrm{K}^0_S \to \pi^+\pi^-$ and from the $\mathrm{K}^{*0}(892)$ reflection. For the ω or $(\eta+\eta')$, x_p is the scaled momentum of their $\pi^+\pi^-$ decay products.

The ρ^0 signal is much better seen in the data for $x_p \geq 0.1$ than for smaller x_p-values. One sees also clearly that for the data integrated over all $\cos\theta^*$ (fig. 11b-f), the signal represents the sum of the real ρ^0 and of the $\mathrm{K}^{*0}(892)$ reflection, so that the ρ^0 contribution can be reliably obtained only when the $\mathrm{K}^{*0}(892)$ cross section is fixed as has been explained above. In spite of a very large combinatorial background, the narrow $f_0(975)$ is observed in the $\pi^+\pi^-$ mass spectra for $x_p \geq 0.05$ even without background subtraction. The relatively broad $f_2(1270)$ is only slightly indicated in the $\pi^+\pi^-$ mass spectra, but is clearer for $x_p \geq 0.05$ after the background subtraction.

The ρ^0, $f_0(975)$ and $f_2(1270)$ differential cross sections obtained from the fit are tabulated in table 3 and shown in fig. 12, with the statistical and systematic errors combined quadratically. In calculating the $f_0(975)$ and $f_2(1270)$ production rates, the unobserved decay modes were taken into account.

The systematic errors for the ρ^0 production rates were estimated by analyzing uncertainties arising from:

1) mass dependence of the factors R which account for the difference between the data and DELSIM when the samples with the weak or strong cuts are used (see Sect. 3);
2) treatment of Bose-Einstein correlations;
3) choice of background parameterization, bin size of the mass spectra and mass range used in the fit.

The relative error from the first factor is 2.2% and is practically independent of x_p. The second contribution was estimated by comparing the ρ^0 cross sections obtained with the adopted treatment of Bose-Einstein correlations with the ones when Bose-Einstein correlations were ignored, but the fits were done with the ρ^0 masses taken at their shifted measured values. For the $\pi^+\pi^-$ invariant mass distribution in the $|\cos\theta^*| \leq 0.25$ region and for the $x_p \geq 0.025$, the corresponding relative error was found to be 9%. However, this systematic uncertainty was found to be a strong function of x_p decreasing from around 20% at the smallest x_p-interval down to zero for the largest x_p- interval, as can be expected. In fact, it can be practically ignored for $x_p \geq 0.1$. This x_p-dependence was taken into account in calculating the systematic errors for the differential cross section. The third contribution was estimated, as in the case of the $\mathrm{K}^{*\pm}(892)$, by applying the same fitting procedure to the events generated by JETSET 7.3 and passed to DELSIM then selected exactly as the real data and comparing the cross sections obtained with the input values. This gave a relative error of 1%. Notice also that some systematic is, in fact, included into the statistical errors obtained from the fit, since the $\mathrm{K}^{*\pm}(892)$, η and η' production rates, ω/ρ^0 ratio and masses and widths from the PDG tables have been taken with their systematic uncertainties.

Similar procedures were applied to estimate the systematic uncertainties on the $f_0(975)$ and $f_2(1270)$ production rates. For the $f_2(1270)$, an additional 20% systematic error was added to account for possible influence of the $K_2^{*0}(1430)$ reflection.

The average ρ^0, $f_0(975)$ and $f_2(1270)$ multiplicities per hadronic Z^0 decay in the measured x_p-regions obtained by integration of their x_p-distributions are presented in table 4. Extrapolation to the full x_p-range for the ρ^0 was made from the measured average multiplicity in the $x_p \geq 0.025$ range:

$$< N(\rho^0) > = 0.98 \pm 0.03(stat) \pm 0.12(syst), \tag{13}$$

assuming the unmeasured region is represented by the normalized JETSET 7.4 PS model (with 20% systematic uncertainty). This gave:

$$< N(\rho^0) > = 1.21 \pm 0.04(stat) \pm 0.14(syst) \pm 0.05(extr). \tag{14}$$

The ρ^0, $f_0(975)$ and $f_2(1270)$ average multiplicities thus obtained update the previous DELPHI measurements based on smaller statistics [17] which agree within errors with the present measurements.

The measured ratio

$$\sigma(f_2(1270))/\sigma(\rho^0) = 0.24 \pm 0.07 \tag{15}$$

for $0.05 \leq x_p \leq 1.0$ agrees with the tensor-to-vector meson ratios measured in hadronic reactions (with an average value of 0.25 ± 0.03), as mentioned in [17].

The measured ratio

$$\sigma(f_2(1270))/\sigma(f_0(975)) = 1.7 \pm 0.5 \tag{16}$$

for $0.05 \leq x_p \leq 0.6$ agrees with the value of 2 ± 1 measured by the HRS collaboration at 29 GeV [11].

6 Discussion and conclusions

The average K^0, $K^{*\pm}(892)$, ρ^0, $f_0(975)$ and $f_2(1270)$ multiplicities measured in this experiment are shown in table 4. For the K^0, $K^{*\pm}(892)$ and ρ^0 these multiplicities were extrapolated to the full x_p-range using the JETSET 7.4 PS model. Table 4 also shows the K^0, $K^{*\pm}(892)$ and ρ^0 multiplicities in the JETSET model with the default (and tuned) values of the parameters. The corresponding differential cross sections $(1/\sigma_h)\cdot d\sigma/dx_p$ are compared with the model expectations in figs. 8 and 12.

The overall measured average K^0 multiplicity is smaller than the model with default parameters by 13%. Figs. 8a and 8b show that this difference results from failure of the model to reproduce quantitatively the measured momentum spectrum at low momenta.

The overall average $K^{*\pm}(892)$ multiplicity predicted by JETSET with default parameters is significantly larger than the measured value. OPAL observes a similar discrepancy [20]. However, the measured $K^{*\pm}(892)$ x_p-spectrum (fig. 8c) agrees well in shape with the predicted one, implying that good agreement between the data and model can be achieved by proper tuning of the JETSET parameters.

The overall average ρ^0 multiplicity is also overestimated by JETSET, but less than in the case of the $K^{*\pm}(892)$. The measured ρ^0 x_p-spectrum (fig. 12) agrees with the predicted one for large x_p-values, but falls slightly below the model expectations for small x_p-values.

For the $f_2(1270)$, a clear tendency for a rise of the $f_2(1270)/\rho^0$ ratio with increasing x_p is seen (fig. 13). This ratio changes from 0.16 ± 0.08 for $0.05 \leq x_p \leq 0.10$ up to 1.1 ± 0.4 for $0.6 \leq x_p \leq 1.0$. The fit of the x_p dependence of the ratio by a form $a \exp(bx_p)$

(straight line in fig. 13) yields $a = 0.14 \pm 0.04$ and $b = 2.4 \pm 0.7$. Only a small part of this effect can be attributed to the mass difference. This was checked by generating the ρ^0 x_p-spectra in JETSET with the ρ^0 masses of 770 and 1270 MeV. Fit of their ratio by the same form resulted in much smaller value of $b = 1.2$ in comparison with the experimental result for the $f_2(1270)/\rho^0$ ratio. The increase of the $f_2(1270)/\rho^0$ ratio with increasing x_p is consistent with hints from hadronic experiments, where the same tendency was observed for the higher tensor-to-vector meson ratio with increase of the scaled momentum [32].

Within the limits of large errors, the $f_0(975)$ and ρ^0 x_p-spectra (fig. 12) have similar shapes. This is also seen from the fit of the $f_0(975)/\rho^0$ ratio by a form $a \exp(bx_p)$ (straight line in fig. 13) which yields $b = 1.2 \pm 0.9$. This indicates rather similar production mechanisms for these mesons. The same observation for the ρ^0 and $f_0(975)$ was recently made by the ARGUS collaboration [14]. It was also noticed in [14] that independence of the relative production rates of $f_0(975)$ and ρ^0 mesons of the centre-of-mass energy can be considered as an additional argument in favour of their similar production mechanisms. The DELPHI value of the ratio

$$f_0(975)/\rho^0 = 0.14 \pm 0.03 \tag{17}$$

for $0.05 \leq x_p \leq 0.6$ might be compared with the values 0.072 ± 0.018, measured for continuum e^+e^--events by ARGUS around $\sqrt{s} = 10$ GeV [14], and 0.063 ± 0.032 measured by HRS at $\sqrt{s} = 29$ GeV [11]. For a study of this ratio as a function of rapidity and separation from other hadrons in phase space as advocated in [4], larger statistics are necessary.

The study of inclusive meson resonance production at LEP energies has shown a number of unexpected features. The $\eta'(958)$ production rate measured by ALEPH [16] was observed to be much lower than predicted by the models. The $\phi(1020)$, $K^{*\pm}(892)$, $K^{*0}(892)$ and ρ^0 production rates measured by OPAL [18,20] and DELPHI also fall significantly below the JETSET model with default parameters. The centre-of-mass energy dependence of the $K^{*\pm}(892)$ and ρ^0 production rates (fig. 14) shows that JETSET 7.4 PS has a stronger rise of the production rates between $\sqrt{s} = 35$ GeV and LEP energies than exhibited by the data. The measured $K^{*\pm}(892)$ average multiplicity at LEP energies is, in particular, surprisingly similar to those observed in e^+e^- collisions at energies around $\sqrt{s} = 35$ GeV, contrary to the expected increase with energy in JETSET.

Since the shapes of the measured and predicted x_p-spectra for the $K^{*\pm}(892)$ and ρ^0 are rather similar, one can easily obtain reasonable agreement between the data and model expectations for the resonance production rates at a given energy by tuning the model parameters responsible for strangeness suppression and for the relative rate of pseudoscalar and vector meson production as, for example, has been done in [18]. Such tuning of the JETSET 7.4 PS to the DELPHI K^0 ξ-spectrum and $K^{*\pm}(892)$ and ρ^0 x_p-spectra gave the following values for the model parameters controlling, respectively, the strangeness suppression and the probabilities that strange or nonstrange mesons will have spin 1: PARJ(2) = 0.230, PARJ(12) = 0.410[¶] and PARJ(11) = 0.365 (to be compared with the default values of 0.3, 0.6 and 0.5). The JETSET 7.4 x_p-spectra thus obtained (dashed curves in figs. 8 and 12) describe the data quite well. The corresponding JETSET 7.4 rates for the K^0, $K^{*\pm}(892)$ and ρ^0 obtained with these parameters are given in table 4. As for the energy dependence of the K^0, $K^{*0\pm}(892)$ and ρ^0 production rates, the model with parameters tuned to the DELPHI data (dashed curves in fig. 14) lies systematially below most of the data at lower energies. Thus it seems doubtful that the model, with only one set of parameters, will be able to describe the measured energy dependence of the particle production rates.

[¶]Not surprisingly, these DELPHI values are very close to the OPAL values of 0.245 and 0.43.

The important $f_0(975)$ and $f_2(1270)$ production rates measured by DELPHI represent another challenge for the JETSET model. It indicates that other resonance states, so far not included in JETSET or other models attempting to describe quark and gluon hadronization, are produced with non-negligible production rates, even if their inclusive production is difficult to measure experimentally. In this case, a much larger fraction of the observed final state particles results from the decay of these numerous resonances than usually assumed. Consequently the relative rate of prompt pseudoscalar and vector mesons might differ significantly from that in JETSET. For these reasons, further precise measurements of meson resonance rates at high statistics LEP experiments are highly desirable.

The significant mass shift observed for the ρ^0 by OPAL [18] and DELPHI requires further investigation. In this paper it was shown that this mass shift is dominantly influenced by the reflection from the $K^{*0}(892)$ and by the residual Bose-Einstein correlations and can be successfully corrected for when these effects are properly taken into account. However other effects, such as $\rho^0 - \omega$ interference and interference with coherent non-resonant $\pi^+\pi^-$ background, can also distort the ρ^0 shape. In particular, the background interference mechanisms can have similar phenomenological effects to those arising from the residual Bose-Einstein correlations [30] It remains to be seen, with still higher statistics to be accumulated by LEP experiments, whether inclusion of these effects will be necessary in order to describe the experimental data.

Acknowledgements

We are greatly indebted to our technical staff and collaborators and funding agencies for their support in building and operating the DELPHI detector, and to the members of the CERN-SL Division for the excellent performance of the LEP collider. We thank T. Sjöstrand for useful discussions on Bose-Einstein correlations in JETSET.

References

[1] B. Andersson et al., Phys. Rep. **97** (1983) 31.
[2] G. C. Fox and S. Wolfram, Nucl. Phys. **B168** (1980) 285.
[3] V. N. Gribov, Lund Preprint LU-TP 91-7 (1991).
[4] F. E. Close et al., Rutherford Report RAL-93-049 (1993).
[5] NA22 Collab., N. M. Agababyan et al., Z. Phys. **C41** (1989) 539; **C46** (1990) 387.
[6] NA27 Collab., M. Aguilar-Benitez et al., Z. Phys. **C44** (1989) 531; **C50** (1991) 405.
[7] TASSO Collab., R. Brandelik et al., Phys. Lett. **B117** (1982) 135.
[8] JADE Collab., W. Bartel et al., Phys. Lett. **B145** (1984) 441.
[9] TPC Collab., H. Aihara et al., Phys. Rev. Lett. **53** (1984) 2378.
[10] CLEO Collab., S. Behrends et al., Phys. Rev. **31** (1985), 2161.
[11] HRS Collab., S. Abachi et al., Phys. Rev. **D40** (1989) 706; Phys. Rev. Lett. **57** (1986) 1990; Phys. Lett. **B199** (1987) 151.
[12] CELLO Collab., H.-J. Behrend et al., Z. Phys. **C46** (1990) 397.
[13] TASSO Collab., R. Braunschweig et al., Z. Phys. **C47** (1990) 167.
[14] ARGUS Collab., L. Albrecht et al., Z. Phys. **C41** (1989) 557; **C58** (1993) 199; **C61** (1994) 1.
[15] L3 Collab., O. Adriani et al., Phys. Lett. **B286** (1992) 403.
[16] ALEPH Collab., D. Buskulic et al., Phys. Lett. **B292** (1992) 210.
[17] DELPHI Collab., P. Abreu et al., Phys. Lett. **B298** (1993) 236.
[18] OPAL Collab., P. D. Acton et al., Z. Phys. **C56** (1992) 521.
[19] DELPHI Collab., P. Abreu et al., Phys. Lett. **B275** (1992) 231.
[20] OPAL Collab., P. D. Acton et al., Phys. Lett. **B305** (1993) 407.
[21] JETSET Monte Carlo program : T. Sjöstrand, Comp. Phys. Comm. **27** (1982) 243; **28** (1983) 229; **39** (1986) 347; T. Sjöstrand and M. Bengtsson, Comp. Phys. Comm. **43** (1987) 367.
[22] DELPHI Collab., P. Aarnio et al., Nucl. Instr. Methods **A303** (1991) 233.
[23] DELSIM User Guide, DELPHI 87-96 PROG-99 (Geneva, July 1989); DELSIM Reference Manual, DELPHI 87-98 PROG-100 (Geneva, July 1989).
[24] V. P. Zhigunov, Nucl. Instr. Meth. **216** (1983) 183; V. V. Ammosov, Z. U. Usubov and V. P. Zhigunov, ibid. **A295** (1990) 224; V. B. Anykeyev, A. A. Spiridonov, V. P. Zhigunov, ibid. **A303** (1991) 350; **A322** (1992) 280.
[25] DELPHI Collab., P. Abreu et al., Z. Phys. **C52** (1991) 52.
[26] Particle Data Group, M. Aguilar-Benitez et al., Phys. Rev. **D45** (1992) 1.
[27] OPAL Collab., G. Alexander et al., Phys. Lett. **B264** (1991) 467.
[28] L3 Collab., G. Acciari et al., Phys. Lett. **B238** (1994) 223.
[29] ALEPH Collab., D. Buskulic et al., CERN-PPE/94-74 (1994).
[30] G.D.Lafferty, Z. Phys. **C60** (1993) 659.
[31] DELPHI Collab., P. Abreu et al., Preprint CERN-PPE/94-02 (1994) (submitted to Z. Phys.C).
[32] NA27 Collab., J.L. Bailly et al., Z. Phys. **C36** (1987) 545.
[33] ARGUS Collab., L. Albrecht et al., Z. Phys. **C44** (1989) 547.
[34] JADE Collab., W. Bartel et al., Z. Phys. **C20** (1983) 87.
[35] MARK II Collab., H. Schellman et al., Phys. Rev. **D31** (1985), 3013.
[36] HRS Collab., M. Derrick et al., Phys. Rev. **D35** (19879) 2639.

Tables

Table 1: Differential cross section for K^0 as a function of ξ and x_p. The differential cross section $(1/\sigma_h)\cdot d\sigma/dx_p$ is calculated at the point $< x_p >$ corresponding to the indicated ξ-interval. The systematic errors are included.

ξ-interval	$(1/\sigma_h)\cdot d\sigma/d\xi$	$< x_p >$	$(1/\sigma_h)\cdot d\sigma/dx_p$
0.0 - 0.6	0.048 $\pm$ 0.020	0.774	0.06 $\pm$ 0.03
0.6 - 0.8	0.138 $\pm$ 0.026	0.499	0.28 $\pm$ 0.05
0.8 - 1.0	0.165 $\pm$ 0.025	0.409	0.40 $\pm$ 0.06
1.0 - 1.2	0.270 $\pm$ 0.027	0.335	0.81 $\pm$ 0.08
1.2 - 1.4	0.338 $\pm$ 0.025	0.274	1.24 $\pm$ 0.09
1.4 - 1.6	0.441 $\pm$ 0.023	0.224	1.97 $\pm$ 0.10
1.6 - 1.8	0.526 $\pm$ 0.024	0.184	2.87 $\pm$ 0.13
1.8 - 2.0	0.558 $\pm$ 0.024	0.150	3.72 $\pm$ 0.16
2.0 - 2.2	0.632 $\pm$ 0.024	0.123	5.15 $\pm$ 0.19
2.2 - 2.4	0.654 $\pm$ 0.024	0.101	6.52 $\pm$ 0.24
2.4 - 2.6	0.660 $\pm$ 0.024	0.082	8.03 $\pm$ 0.30
2.6 - 2.8	0.679 $\pm$ 0.025	0.068	10.09 $\pm$ 0.37
2.8 - 3.0	0.620 $\pm$ 0.024	0.055	11.25 $\pm$ 0.43
3.0 - 3.2	0.584 $\pm$ 0.024	0.045	12.94 $\pm$ 0.52
3.2 - 3.4	0.583 $\pm$ 0.024	0.037	15.79 $\pm$ 0.66
3.4 - 3.6	0.531 $\pm$ 0.024	0.030	17.56 $\pm$ 0.78
3.6 - 3.8	0.468 $\pm$ 0.023	0.025	18.91 $\pm$ 0.94
3.8 - 4.0	0.410 $\pm$ 0.023	0.020	20.2 $\pm$ 1.1
4.0 - 4.2	0.394 $\pm$ 0.022	0.017	23.7 $\pm$ 1.4
4.2 - 4.4	0.298 $\pm$ 0.020	0.014	21.9 $\pm$ 1.5
4.4 - 4.6	0.232 $\pm$ 0.018	0.011	20.8 $\pm$ 1.6
4.6 - 4.8	0.176 $\pm$ 0.013	0.009	19.3 $\pm$ 1.5
4.8 - 5.0	0.116 $\pm$ 0.010	0.007	15.6 $\pm$ 1.4
5.0 - 5.2	0.077 $\pm$ 0.007	0.006	12.7 $\pm$ 1.2
5.2 - 5.4	0.045 $\pm$ 0.006	0.005	8.9 $\pm$ 1.2
5.4 - 5.6	0.032 $\pm$ 0.004	0.004	7.7 $\pm$ 1.0

Table 2: Differential cross section for $K^{*\pm}(892)$ as a function of x_p. The quoted errors are respectively statistical (obtained from the fit) and systematic.

x_p-interval	$(1/\sigma_h)\cdot d\sigma/dx_p$
0.05-0.10	2.87 $\pm$ 0.23 $\pm$ 0.13
0.10-0.15	1.86 $\pm$ 0.16 $\pm$ 0.09
0.15-0.20	1.28 $\pm$ 0.14 $\pm$ 0.06
0.20-0.30	0.74 $\pm$ 0.08 $\pm$ 0.03
0.30-0.40	0.41 $\pm$ 0.07 $\pm$ 0.02
0.40-0.60	0.23 $\pm$ 0.04 $\pm$ 0.01

Table 3: Differential cross sections $(1/\sigma_h)\cdot \mathrm{d}\sigma/\mathrm{d}x_p$ for ρ^0, $f_0(975)$ and $f_2(1270)$ as a function of x_p. The quoted errors are respectively statistical (obtained from the fit) and systematic.

x_p-interval	ρ^0	$f_0(975)$	$f_2(1270)$
0.025-0.05	10.5 $\pm$ 0.8 $\pm$ 2.1	-	-
0.05-0.10	5.24 $\pm$ 0.37 $\pm$ 0.93	0.79 $\pm$ 0.16 $\pm$ 0.07	0.82 $\pm$ 0.29 $\pm$ 0.18
0.10-0.20	2.56 $\pm$ 0.14 $\pm$ 0.12	0.27 $\pm$ 0.07 $\pm$ 0.02	0.69 $\pm$ 0.13 $\pm$ 0.16
0.20-0.35	0.93 $\pm$ 0.06 $\pm$ 0.04	0.11 $\pm$ 0.03 $\pm$ 0.01	0.21 $\pm$ 0.06 $\pm$ 0.05
0.35-0.60	0.21 $\pm$ 0.02 $\pm$ 0.01	0.057$\pm$ 0.013$\pm$ 0.006	0.09 $\pm$ 0.02 $\pm$ 0.02
0.6-1.0	0.018 $\pm$ 0.005 $\pm$ 0.001	0.003 $\pm$ 0.003 $\pm$ 0.001	0.019 $\pm$ 0.006 $\pm$ 0.001

Table 4: Average particle multiplicities per hadronic event measured in the indicated x_p-region in comparison with the JETSET 7.4 PS model with default parameters and with parameters PARJ(2), PARJ(11) and PARJ(12) tuned to the DELPHI data as described in the text.

x_p-range	Particle	Multiplicity	JETSET (default)	JETSET (tuned)
0-1	K^0	1.962 $\pm$ 0.060	2.21	1.965
0.05-0.60	$\mathrm{K}^{*\pm}(892)$	0.462 $\pm$ 0.029	0.72	0.484
0-1	$\mathrm{K}^{*\pm}(892)$	0.712 $\pm$ 0.067	1.11	0.716
0.025-1.0	ρ^0	0.98 $\pm$ 0.12	1.22	1.04
0-1	ρ^0	1.21 $\pm$ 0.15	1.51	1.28
0.05-0.6	$f_0(975)$	0.098 $\pm$ 0.016	-	-
0.05-0.6	$f_2(1270)$	0.163 $\pm$ 0.041	-	-
0.05-1.0	$f_2(1270)$	0.170 $\pm$ 0.043	-	-

Figure captions

Fig. 1. Plot of the true against measured $K^0_S\pi^\pm$ invariant masses in several x_p-intervals obtained from the simulated events in DELSIM, from which the smearing matrices S_{mn} are obtained.

Fig. 2. The $K^0_S\pi^\pm$ invariant mass dependence of the coefficients A for several x_p-intervals for the simulated events in DELSIM.

Fig. 3. The $\pi^+\pi^-$ invariant mass dependence of the coefficients A for several x_p-intervals for the simulated events in DELSIM.

Fig. 4. The $K^0_S\pi^\pm$ invariant mass dependence of the coefficients C for several x_p-intervals for the simulated events in DELSIM for event samples with the weak and strong cuts.

Fig. 5. The $\pi^+\pi^-$ invariant mass dependence of the coefficients C for several x_p-intervals for the simulated events in DELSIM for event samples with the weak and strong cuts.

Fig. 6. The ρ^0 signal and reflection from $K^{*0}(892)$ as generated by JETSET 7.4 PS in different intervals of $\cos\theta^*$. Each distribution is normalized to 1.

Fig. 7. The $\pi^+\pi^-$ invariant mass spectrum for the K^0_S candidates used in the determination of the K^0 cross section. N is the number of events in the given mass interval and N_h the total number of hadronic Z^0 decays.

Fig. 8. Differential cross section for K^0 production as a function of a) ξ and b) x_p, and for c) $K^{*\pm}(892)$ production as a function of x_p. Solid and dashed curves represent the expectations of JETSET 7.4 PS model with default parameters and, respectively, with parameters tuned to the DELPHI data as described in the text.

Fig. 9. The $K^0_S\pi^\pm$ invariant mass spectra for indicated x_p-intervals for the uncorrected data. The histograms are the result of the fit (with indicated values of χ^2/NDF) using function (7). The background is shown by dotted histograms. The lower parts of the figures present the data and the results of the fit after background subtraction.

Fig. 10. Two-pion phase space functions for the ρ^0 with Bose-Einstein correlations taken into account (W) or not (PS) as a function of $M - M_{\rho^0}$ for several x_p-intervals.

Fig. 11. The $\pi^+\pi^-$ invariant mass spectra a) for $|\cos\theta^*| \leq 0.25$ and $x_p \geq 0.025$ and b-f) for five indicated x_p-intervals (for all $\cos\theta^*$-region) for the uncorrected data. The histograms show the result of the fit using the function (7). The background is shown by the dotted histograms. The lower parts of the figures present the data and the results of the fit after background subtraction. Separate contributions from the $\eta + \eta'$, K^0_S, ω decays and the $K^{*0}(892)$ reflection are also shown.

Fig. 12. Differential cross sections $(1/\sigma_h)\mathrm{d}\sigma/\mathrm{d}x_p$ for inclusive ρ^0, $f_0(975)$ and $f_2(1270)$ production. Solid and dashed curves represent the expectations of JETSET 7.4 PS model for the ρ^0 with default parameters and, respectively, with parameters tuned to the DELPHI data as described in the text.

Fig. 13. The $f_2(1270)/\rho^0$ and $f_0(975)/\rho^0$ ratios as a function of x_p. The lines show the results of the fits described in the text.

Fig. 14. The dependence of the a) K^0, b) $K^{*\pm}(892)$ and c) ρ^0 average multiplicities per hadronic event in e^+e^- collisions on the centre-of-mass energy $\sqrt{s}$ in comparison with the expectations of the JETSET 7.4 PS model with default parameters (solid curve) and with parameters tuned to the DELPHI data (dashed curve) as described in the text. Other data are from refs. [7]-[14], [18,20,27,28], [33]-[36]. For ARGUS [14] and CLEO [10] experiments only multiplicities measured in continuum events at 10.45 GeV are given.

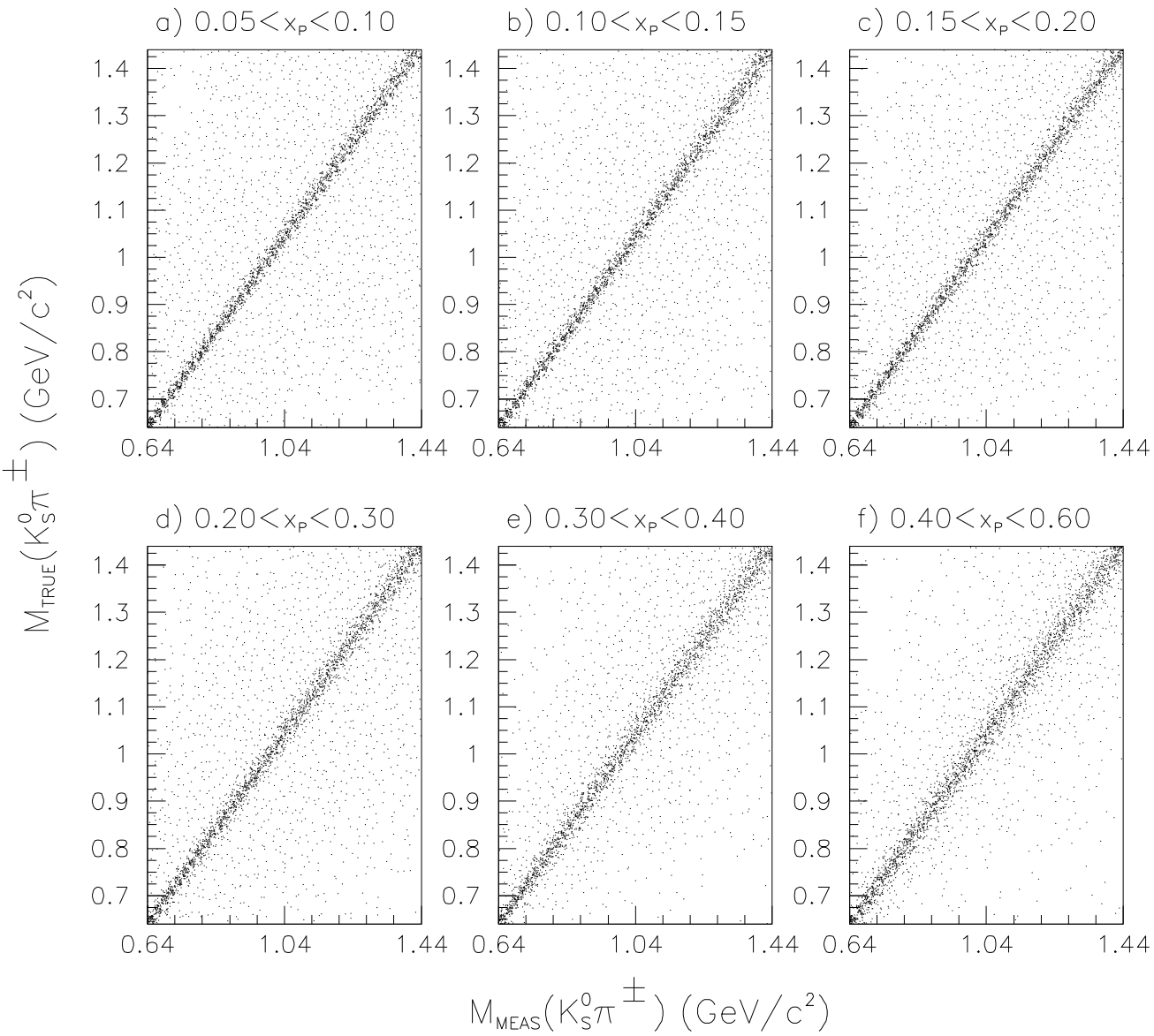
a) 0.05<x_P<0.10
b) 0.10<x_P<0.15
c) 0.15<x_P<0.20
d) 0.20<x_P<0.30
e) 0.30<x_P<0.40
f) 0.40<x_P<0.60
M_TRUE(K⁰_S π^±) (GeV/c²)
M_MEAS(K⁰_S π^±) (GeV/c²)
0.64
1.04
1.44
0.7
0.8
0.9
1
1.1
1.2
1.3
1.4

Fig. 1

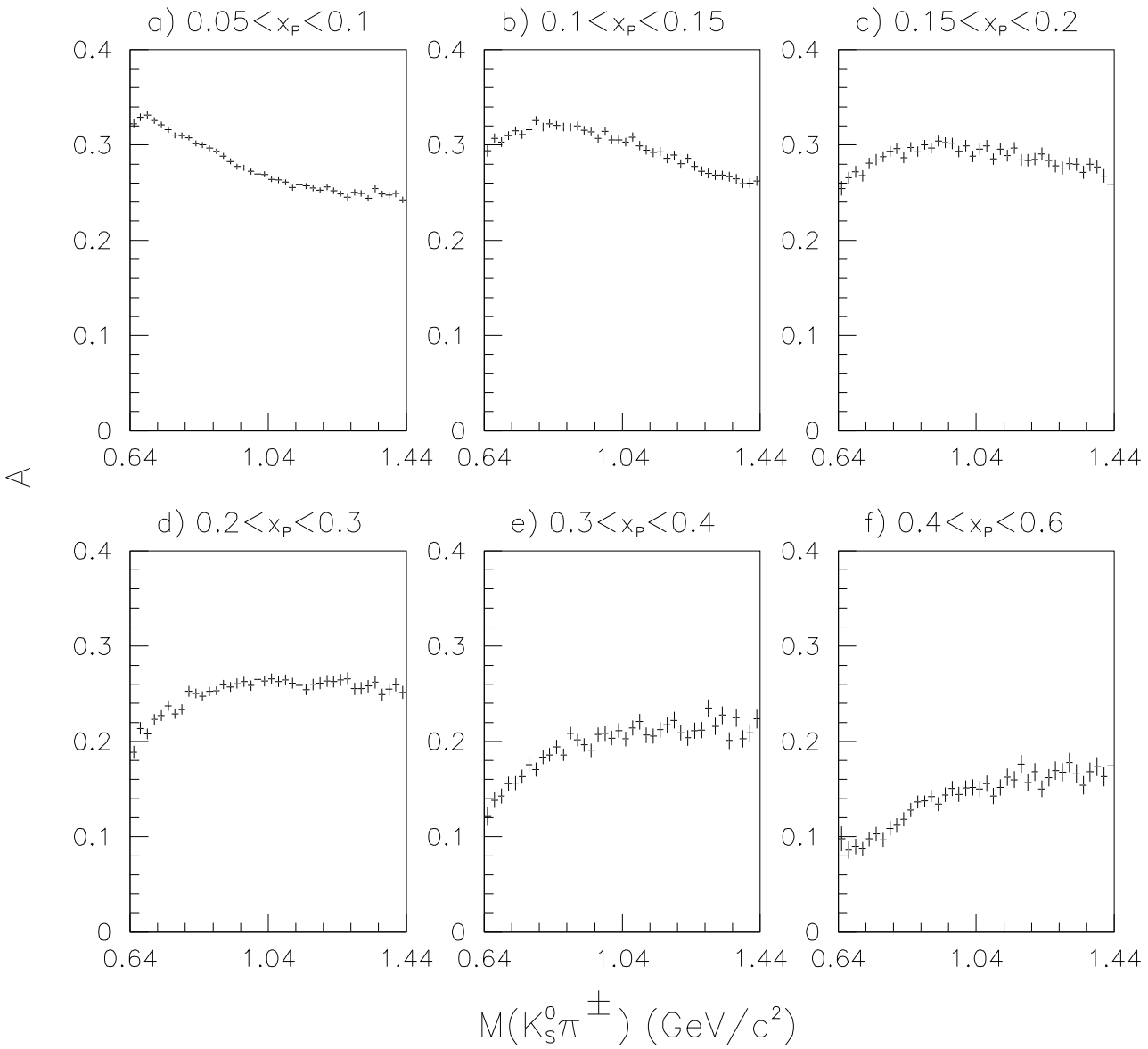
a) 0.05<x_P<0.1
b) 0.1<x_P<0.15
c) 0.15<x_P<0.2
d) 0.2<x_P<0.3
e) 0.3<x_P<0.4
f) 0.4<x_P<0.6
A
M(K⁰_S π^±) (GeV/c²)
0.64
1.04
1.44
0
0.1
0.2
0.3
0.4

Fig. 2

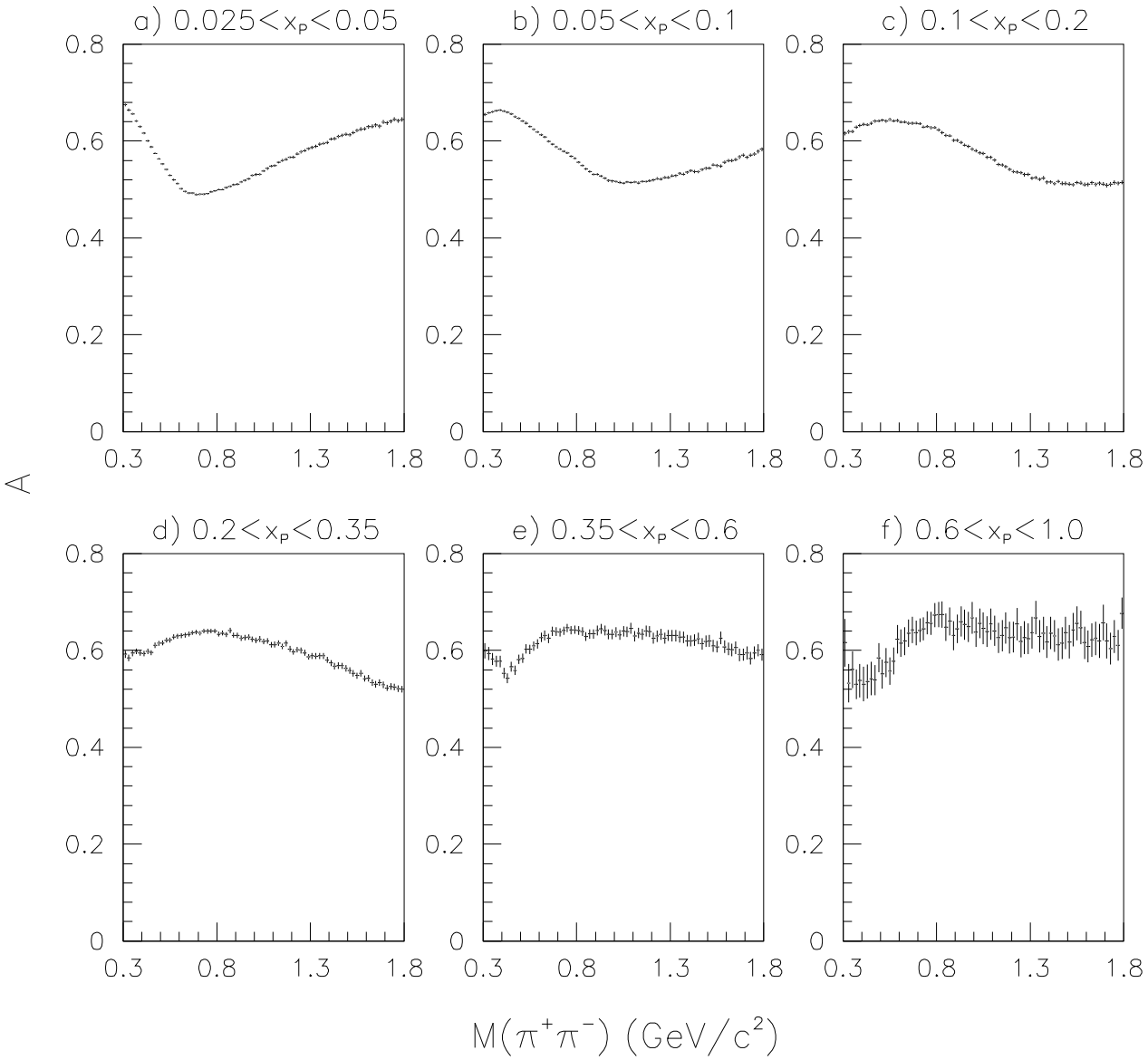
a) 0.025<x_P<0.05
b) 0.05<x_P<0.1
c) 0.1<x_P<0.2
d) 0.2<x_P<0.35
e) 0.35<x_P<0.6
f) 0.6<x_P<1.0
A
M(π⁺π⁻) (GeV/c²)
0
0.2
0.4
0.6
0.8
0.3
0.8
1.3
1.8

Fig. 3

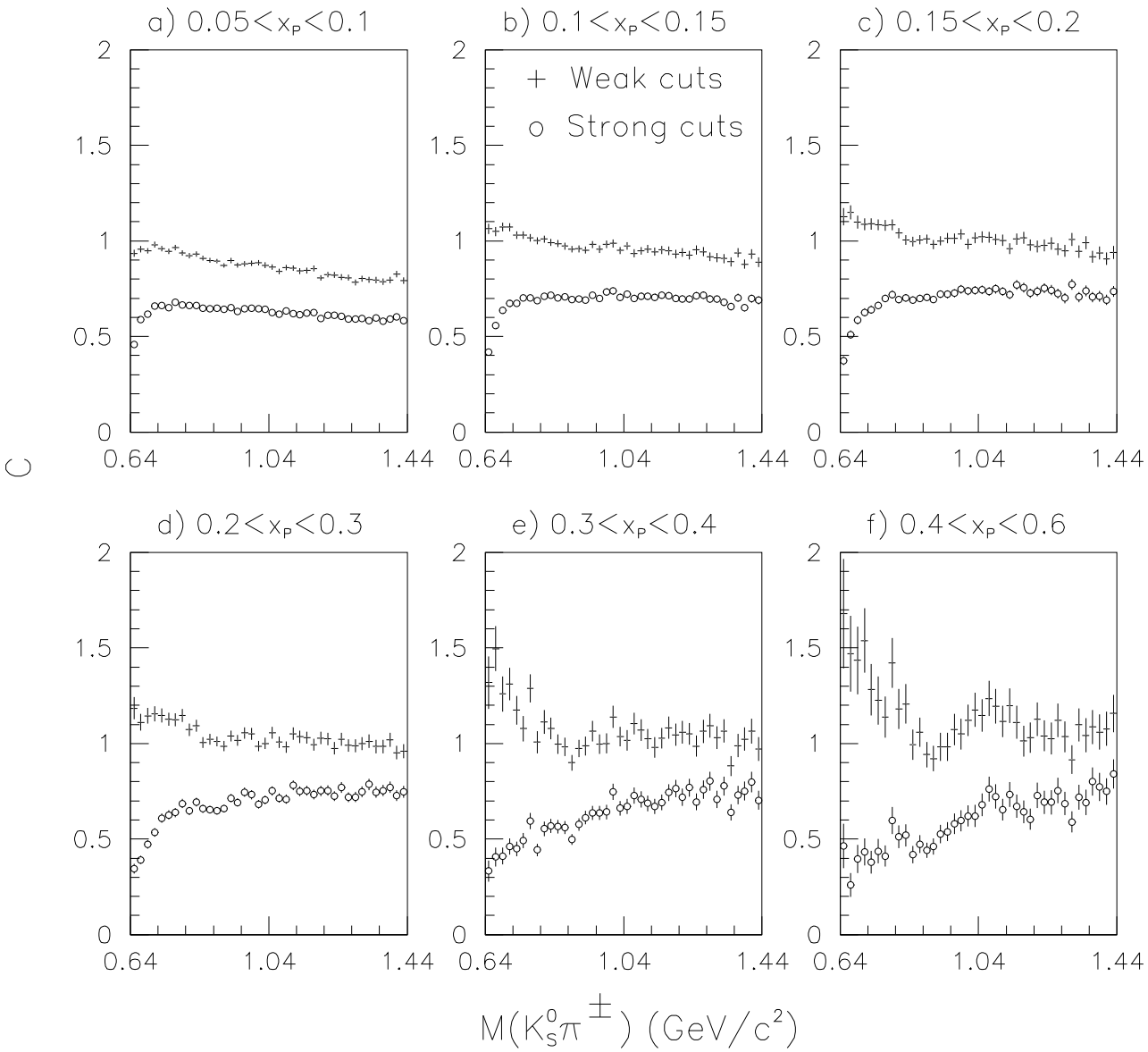
a) 0.05<x_P<0.1
b) 0.1<x_P<0.15
c) 0.15<x_P<0.2
d) 0.2<x_P<0.3
e) 0.3<x_P<0.4
f) 0.4<x_P<0.6
+ Weak cuts
o Strong cuts
C
M(K⁰_S π^±) (GeV/c²)

Fig. 4

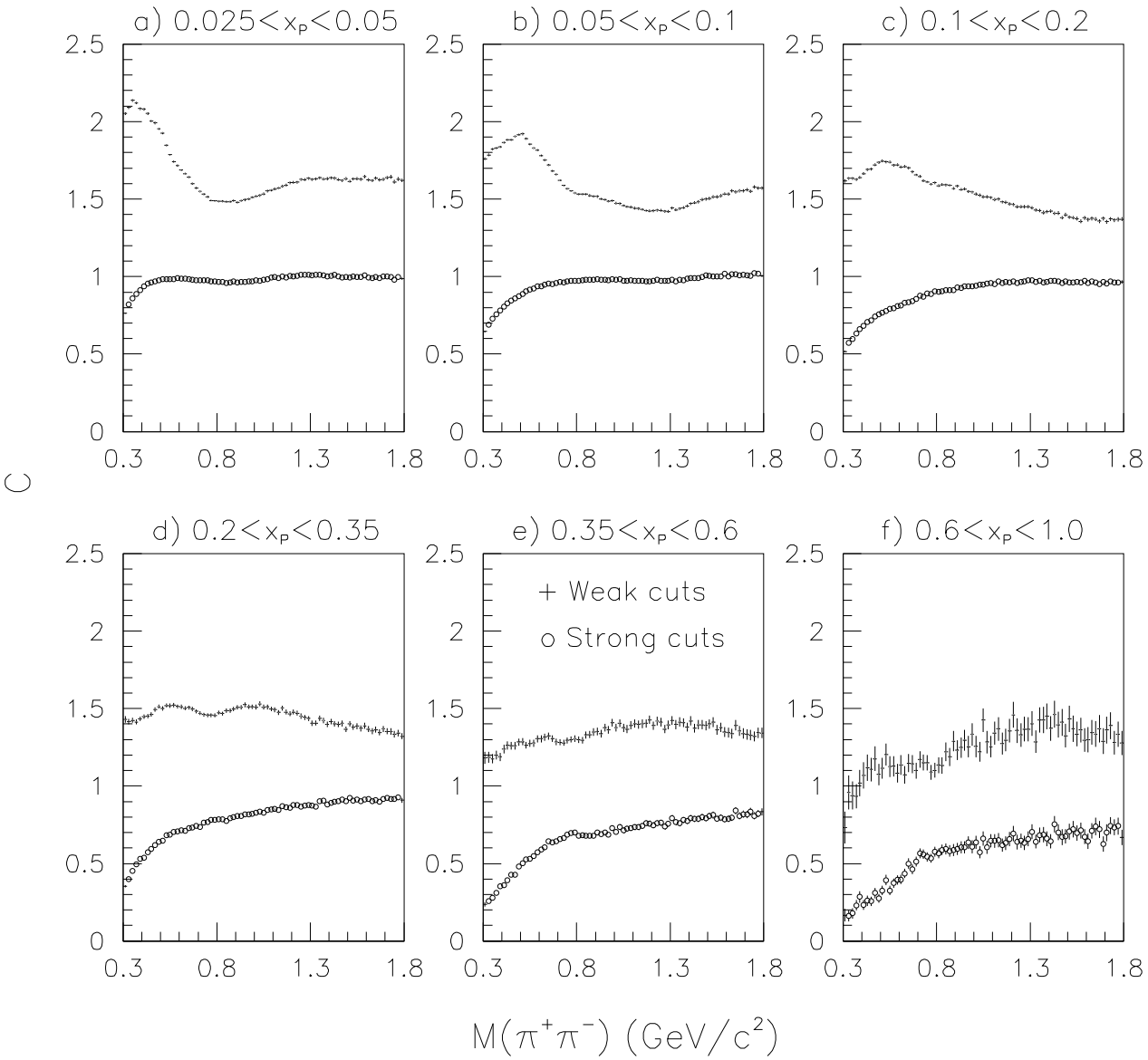
a) 0.025<x_P<0.05
b) 0.05<x_P<0.1
c) 0.1<x_P<0.2
d) 0.2<x_P<0.35
e) 0.35<x_P<0.6
f) 0.6<x_P<1.0
+ Weak cuts
o Strong cuts
C
M(π⁺π⁻) (GeV/c²)

Fig. 5

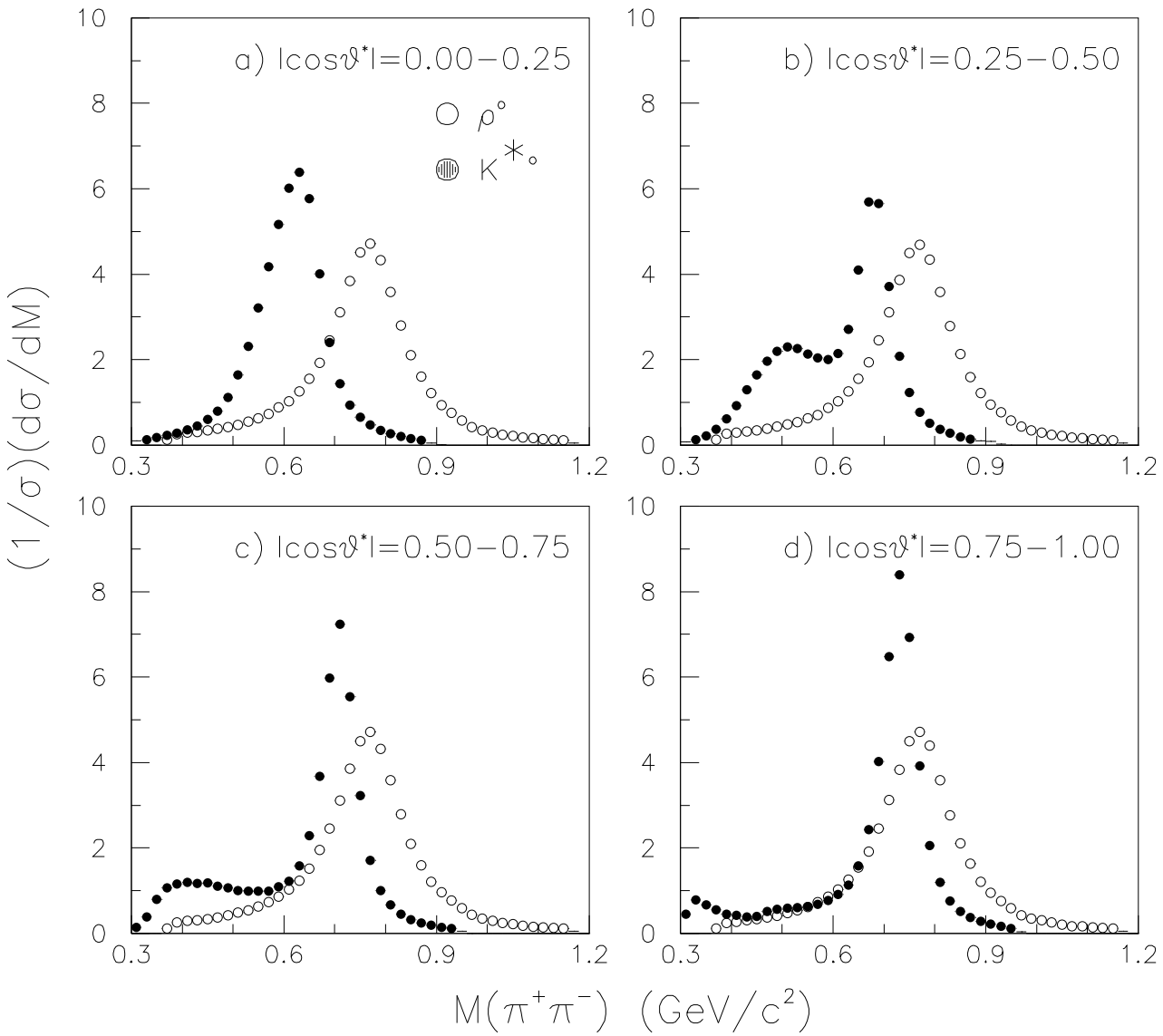
a) |cosϑ*|=0.00−0.25
○ ρ°
◍ K*°
b) |cosϑ*|=0.25−0.50
c) |cosϑ*|=0.50−0.75
d) |cosϑ*|=0.75−1.00
(1/σ)(dσ/dM)
M(π⁺π⁻) (GeV/c²)
0
2
4
6
8
10
0.3
0.6
0.9
1.2

Fig. 6

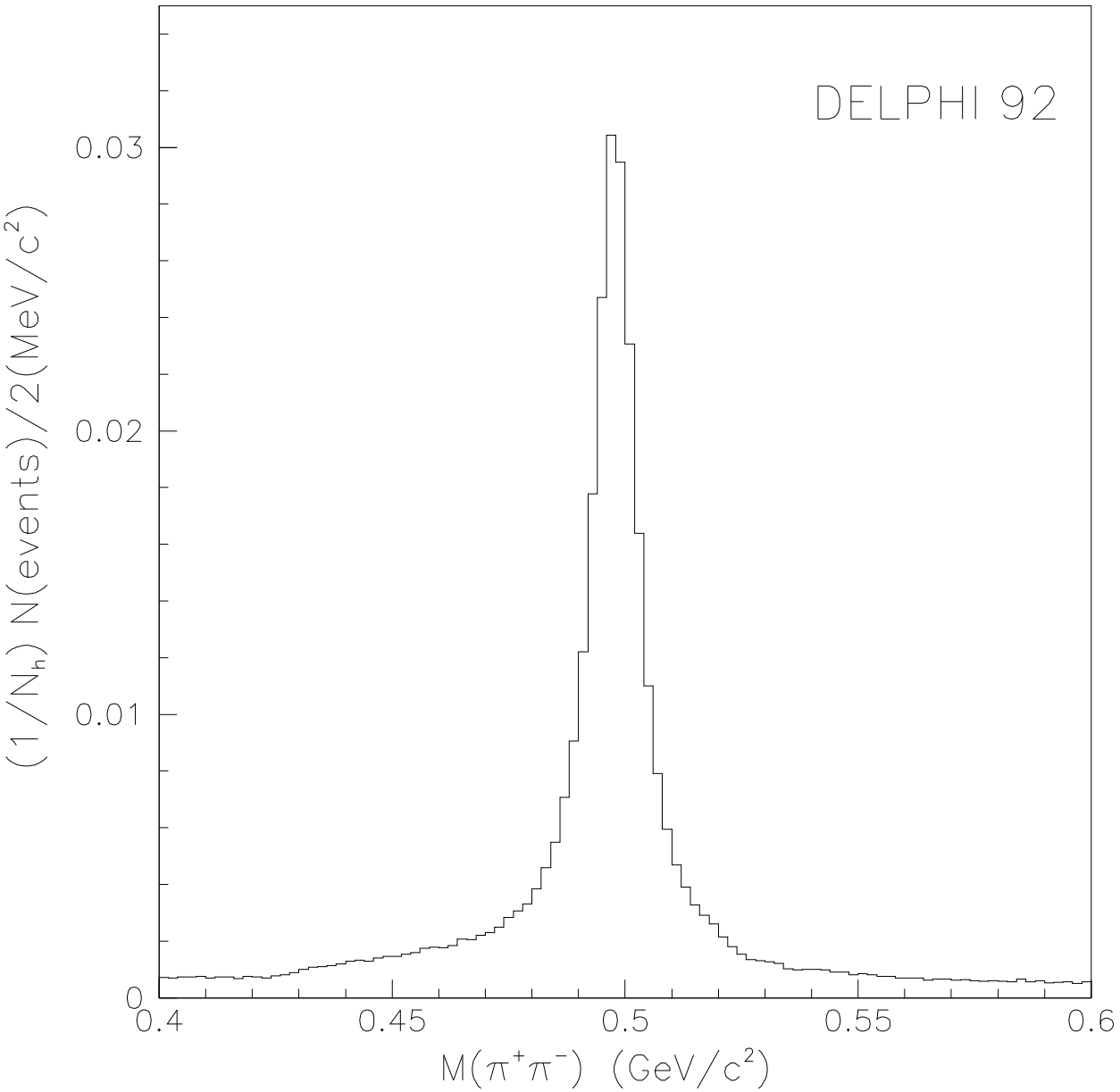
DELPHI 92
0.03
0.02
0.01
0
0.4
0.45
0.5
0.55
0.6
(1/N_h) N(events)/2(MeV/c²)
M(π⁺π⁻) (GeV/c²)

Fig. 7

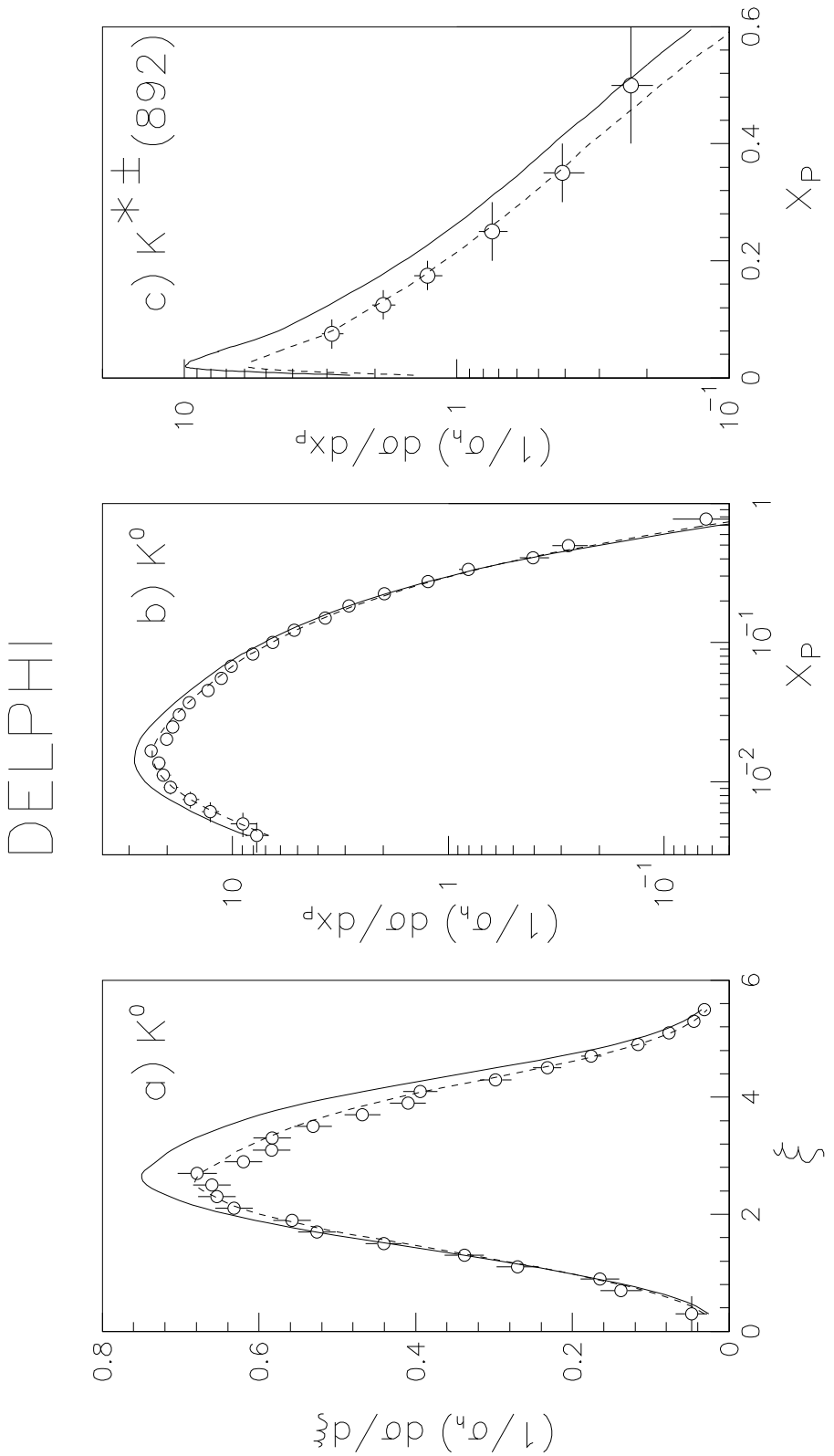

Fig. 8

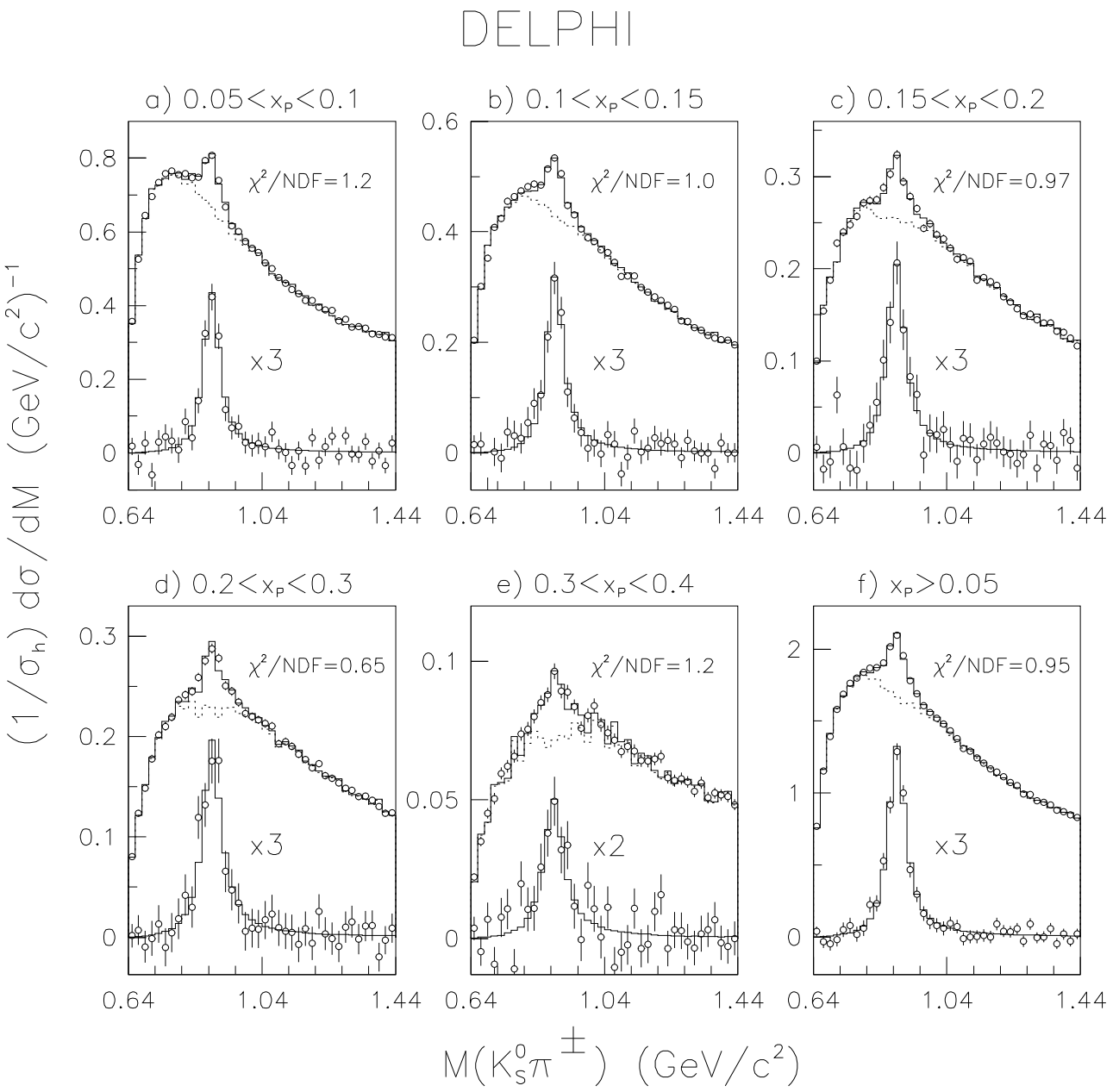
DELPHI
a) 0.05<x_P<0.1
b) 0.1<x_P<0.15
c) 0.15<x_P<0.2
d) 0.2<x_P<0.3
e) 0.3<x_P<0.4
f) x_P>0.05
χ²/NDF=1.2
χ²/NDF=1.0
χ²/NDF=0.97
χ²/NDF=0.65
χ²/NDF=1.2
χ²/NDF=0.95
x3
x2
(1/σ_h) dσ/dM (GeV/c²)⁻¹
M(K⁰_S π±) (GeV/c²)

Fig. 9

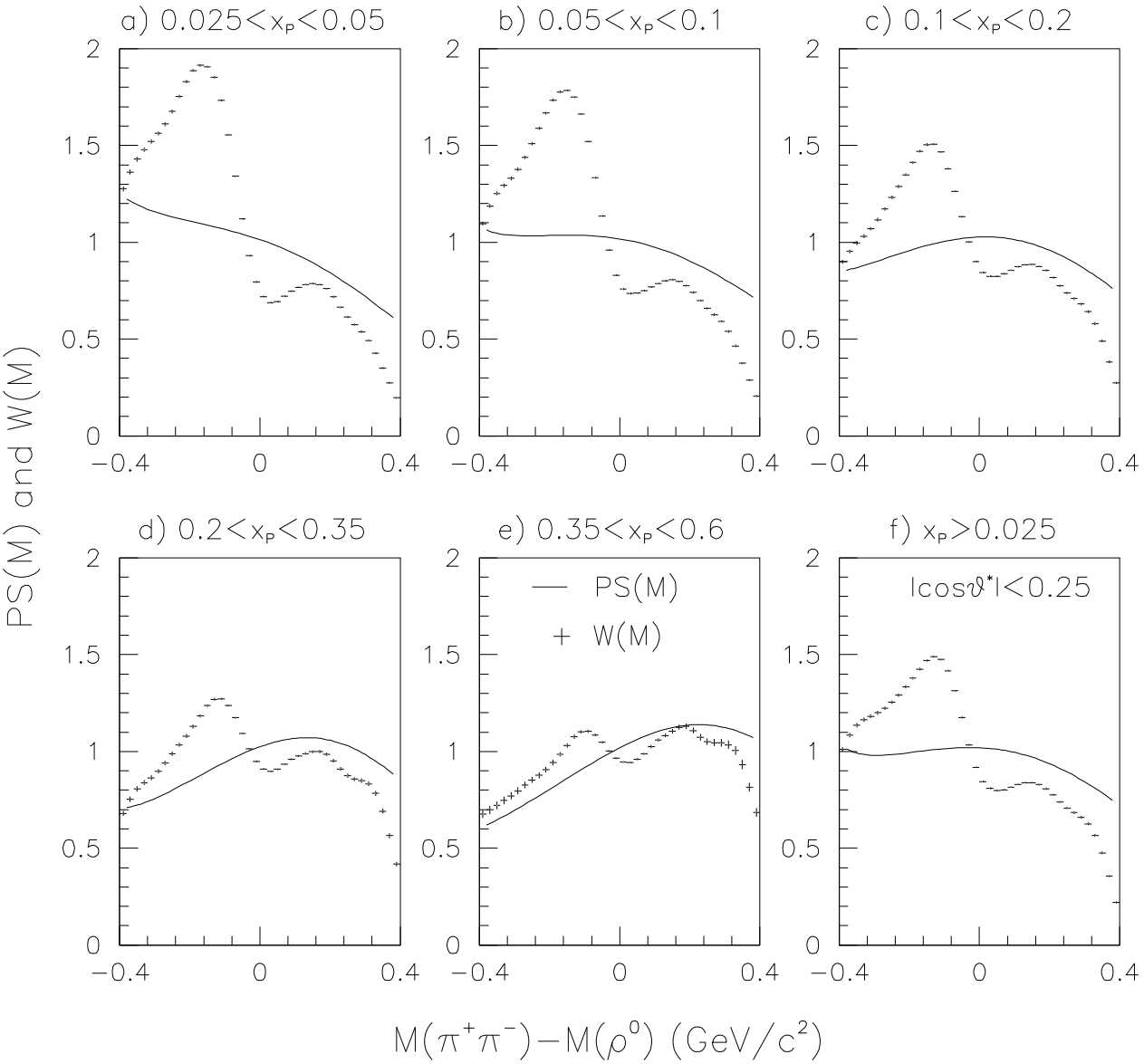
a) 0.025<x_P<0.05
b) 0.05<x_P<0.1
c) 0.1<x_P<0.2
d) 0.2<x_P<0.35
e) 0.35<x_P<0.6
f) x_P>0.025
PS(M)
W(M)
|cosϑ*|<0.25
PS(M) and W(M)
M(π⁺π⁻)−M(ρ⁰) (GeV/c²)

Fig. 10

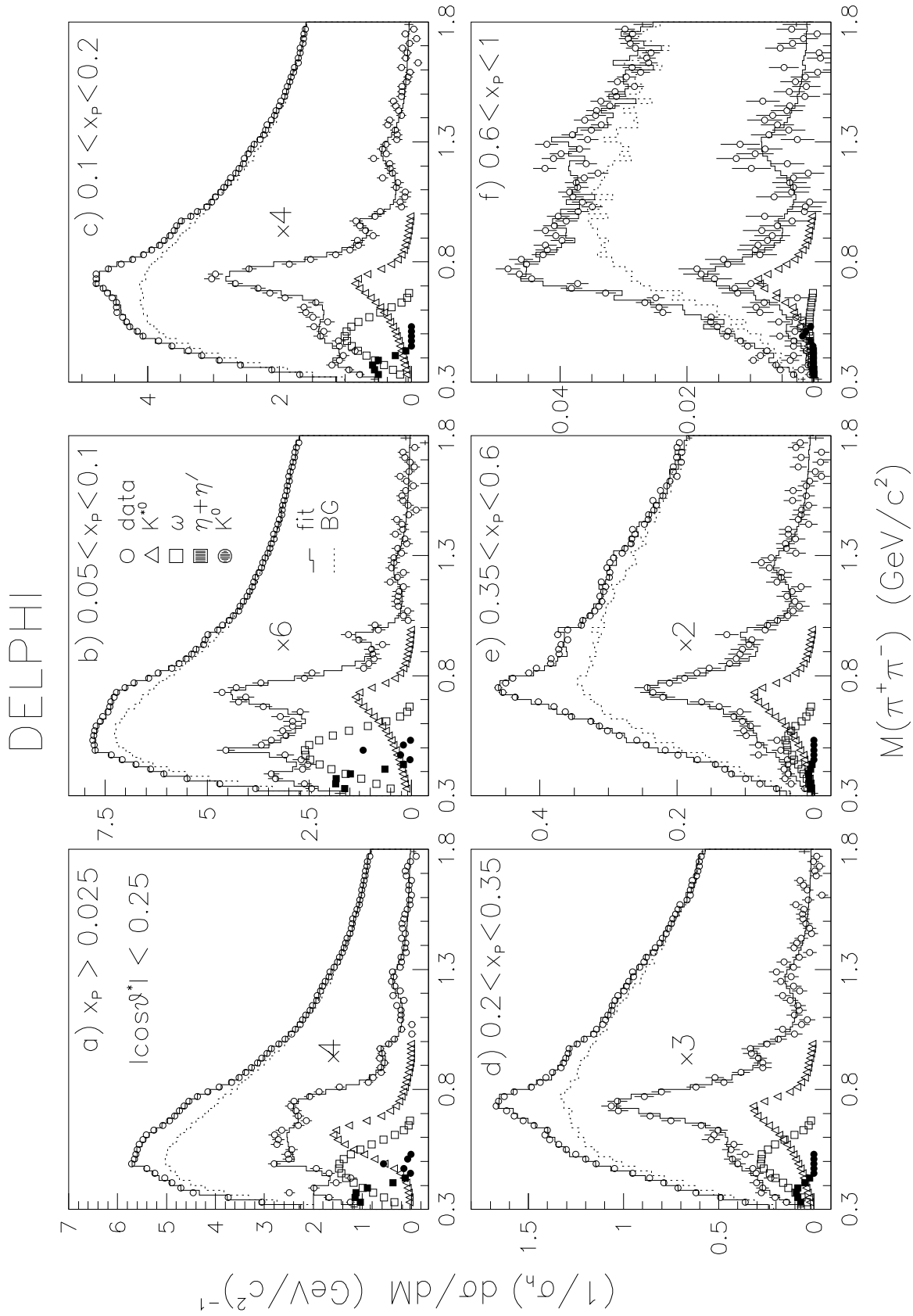
DELPHI
a) $x_P > 0.025$ $|\cos\vartheta^*| < 0.25$
b) $0.05 < x_P < 0.1$
c) $0.1 < x_P < 0.2$
d) $0.2 < x_P < 0.35$
e) $0.35 < x_P < 0.6$
f) $0.6 < x_P < 1$
data
K^{*0}
ω
$\eta+\eta'$
K^0_0
fit
BG
x4
x6
x4
x3
x2
$(1/\sigma_h)\ d\sigma/dM\ (GeV/c^2)^{-1}$
$M(\pi^+\pi^-)\ (GeV/c^2)$

Fig. 11

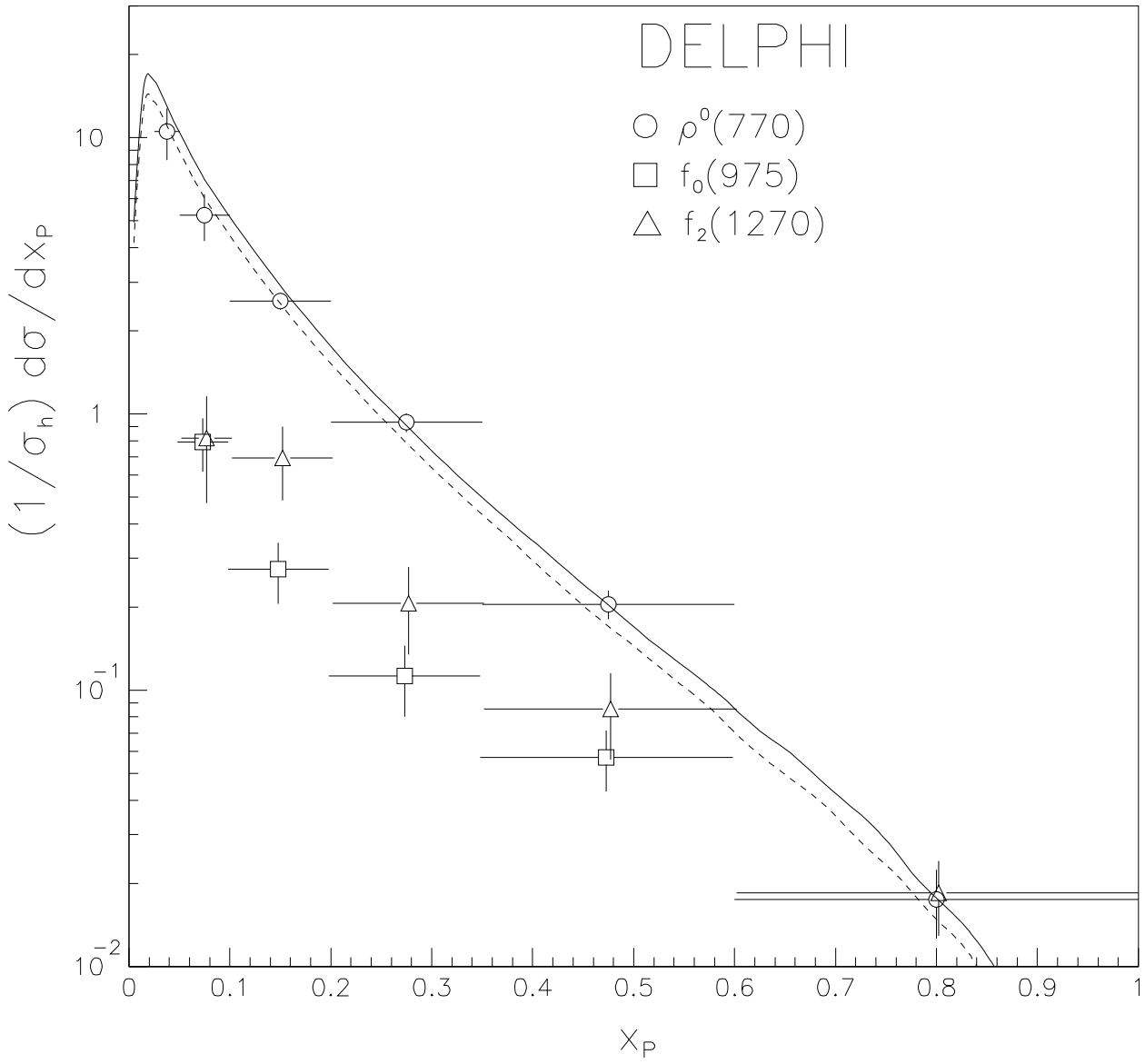
DELPHI
ρ⁰(770)
f₀(975)
f₂(1270)
(1/σh) dσ/dXP
XP
10
1
10⁻¹
10⁻²
0
0.1
0.2
0.3
0.4
0.5
0.6
0.7
0.8
0.9
1

Fig. 12

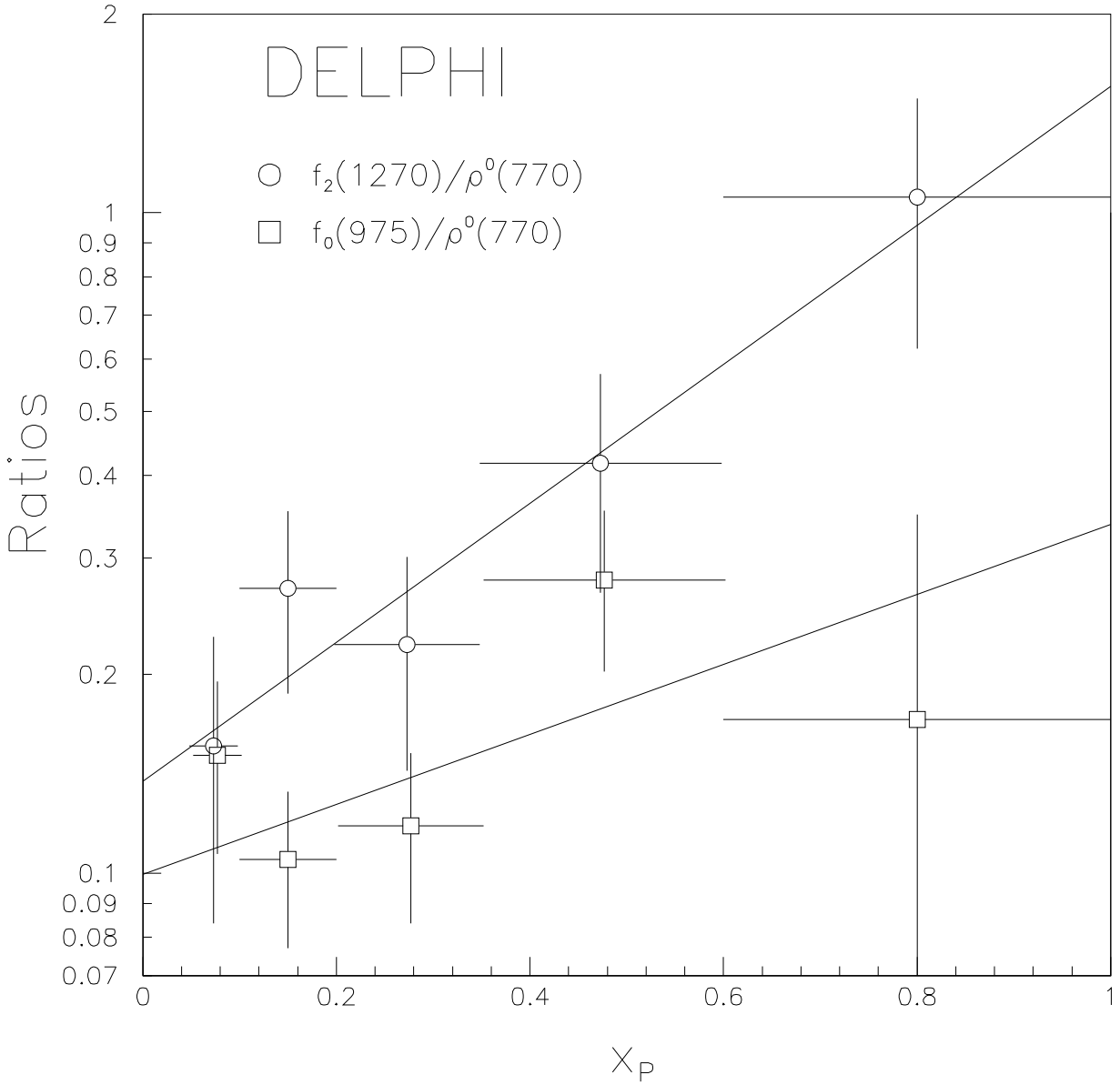
DELPHI
$f_2(1270)/\rho^0(770)$
$f_0(975)/\rho^0(770)$
Ratios
X_P
2
1
0.9
0.8
0.7
0.6
0.5
0.4
0.3
0.2
0.1
0.09
0.08
0.07
0
0.2
0.4
0.6
0.8
1

Fig. 13

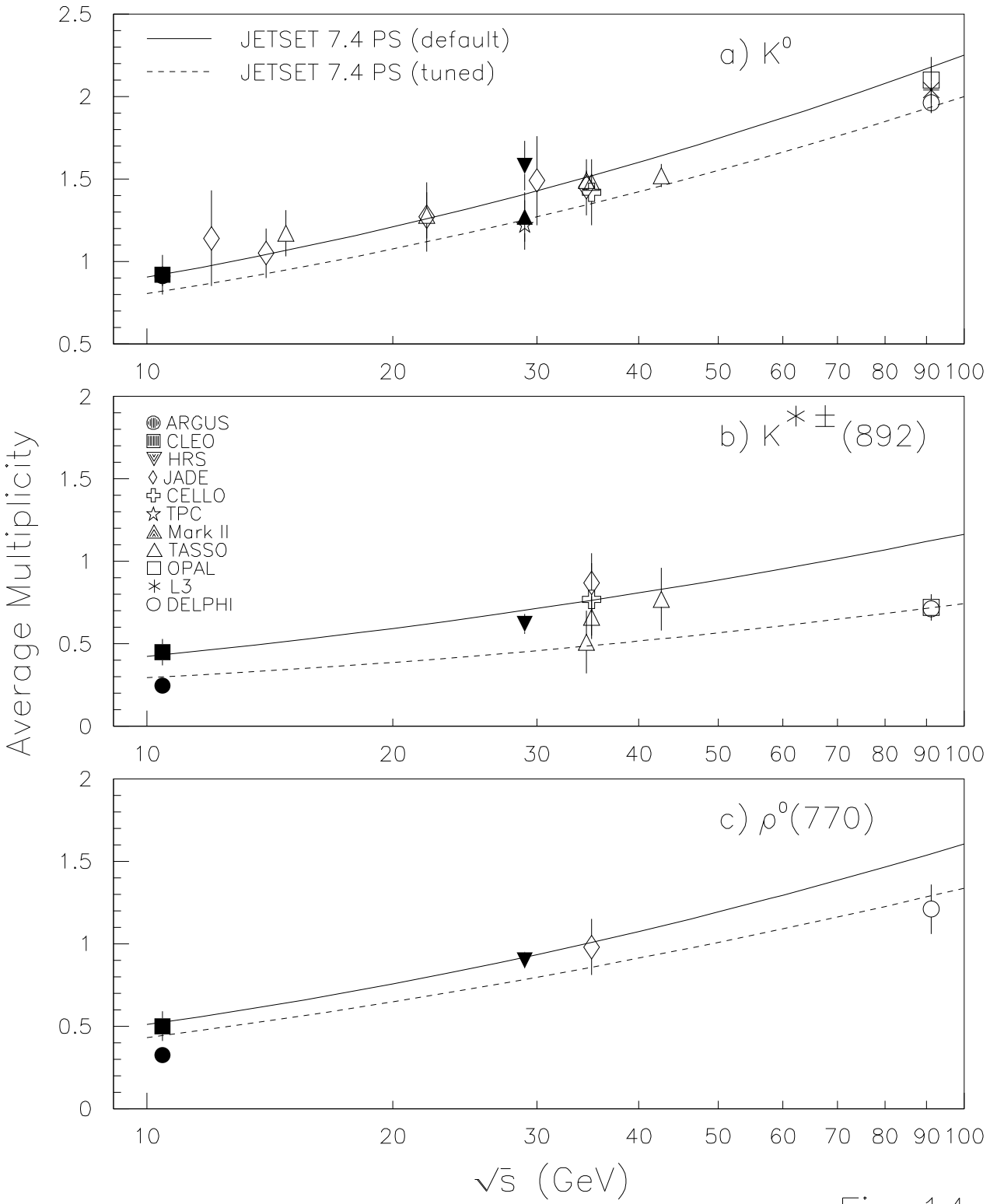
JETSET 7.4 PS (default)
JETSET 7.4 PS (tuned)
a) K⁰
b) K*±(892)
c) ρ⁰(770)
ARGUS
CLEO
HRS
JADE
CELLO
TPC
Mark II
TASSO
OPAL
L3
DELPHI
Average Multiplicity
√s (GeV)

Fig. 14